Simulation and Prototyping of a Knee Assistive Device for Improved Gait Function

Mr. Khemwutta Pornpipatsakul

A Thesis Submitted in Partial Fulfillment of the Requirements
for the Degree of Master of Engineering in Mechanical Engineering
Department of Mechanical Engineering
FACULTY OF ENGINEERING
Chulalongkorn University
Academic Year 2022

การจำลองและการสร้างต้นแบบของอุปกรณ์ช่วยเข่าเพื่อปรับปรุงการทำงานของการเดิน

นายเขมวุฒา พรพิพัฒน์สกุล

วิทยานิพนธ์นี้เป็นส่วนหนึ่งของการศึกษาตามหลักสูตรปริญญาวิศวกรรมศาสตรมหาบัณฑิต
สาขาวิชาวิศวกรรมเครื่องกล ภาควิชาวิศวกรรมเครื่องกล
คณะวิศวกรรมศาสตร์ จุฬาลงกรณ์มหาวิทยาลัย
ปีการศึกษา 2565

Thesis Title	Simulation and Prototyping of a Knee Assistive Device for Improved Gait Function
By	Mr. Khemwutta Pornpipatsakul
Field of Study	Mechanical Engineering
Thesis Advisor	NOPDANAI AJAVAKOM

Accepted by the FACULTY OF ENGINEERING, Chulalongkorn University in Partial Fulfillment of the Requirement for the Master of Engineering

.... Dean of the FACULTY OF ENGINEERING
(SUPOT TEACHAVORASINSKUN)

THESIS COMMITTEE

.... Chairman
(RATCHATIN CHANCHAROEN)

.... Thesis Advisor
(NOPDANAI AJAVAKOM)

.... Examiner
(CHANAT RATANASUMAWONG)

.... External Examiner
(Kakanand Srungboonmee)

เขมวุฒา พรพิพัฒน์สกุล : การจำลองและการสร้างต้นแบบของอุปกรณ์ช่วยเข่าเพื่อปรับปรุงการทำงานของการเดิน. (Simulation and Prototyping of a Knee Assistive Device for Improved Gait Function) อ.ที่ปรึกษาหลัก : นภดนัย อาชวาคม

การวิจัยนี้มุ่งเน้นการพัฒนาอุปกรณ์เสริมกำลังหัวเข่าในระหว่างการเดิน โดยสามารถแบ่งงานวิจัยเป็นสองส่วน คือการคำนวณจำลองในคอมพิวเตอร์ และการสร้างตัวอย่างอุปกรณ์เสริมกำลัง ข้อมูลเกี่ยวกับตำแหน่งของส่วนต่าง ๆ ของร่างกายและแรงตอบสนองที่พื้นถูกเก็บรวบรวมจากผู้เข้าร่วม 3 คน โดยพวกเขาเดินด้วยความเร็ว 1.5 เมตรต่อวินาที เพื่อคำนวณแรงบิดของเข่า ในส่วนของการคำนวณจำลองในคอมพิวเตอร์จะใช้วิธี เทคนิคการควบคุมด้วยปัญญาประดิษฐ์และความยืดหยุ่นเสมือน (MLASCS) ซึ่งประกอบด้วยปัญญาประดิษฐ์ชนิด kNN และสมการความยืดหยุ่นเสมือนต่อน้ำหนัก (IASPB) เพื่อให้การสนับสนุนแรงบิดรอบหัวเข่าเกิดขึ้นในระหว่างการเดิน โดย MLASCS จะถูกนำมาใช้ในการกำหนดปริมาณของการสนับสนุนที่เหมาะสมสำหรับการช่วยเดิน ซึ่งจากการตรวจสอบผลการทดสอบด้วยข้อมูลที่บันทึกไว้แสดงให้เห็นว่า การใช้ MLASCS สามารถลดการออกแรงได้ถึง 63.4% อนึ่งในส่วนของการสร้างตัวอย่างอุปกรณ์เสริมกำลัง อุปกรณ์จะถูกออกแบบและสร้างโดยการใช้เทคโนโลยีการพิมพ์ 3 มิติ ซึ่งได้ถูกทดสอบความคงทนของอุปกรณ์หลังการผลิตแล้ว ระบบควบคุมของตัวอย่างอุปกรณ์นี้จะใช้เครื่องส่งกำลังที่ถอดแบบมาจากเซอร์โวมอเตอร์รุ่น MIT mini-cheetah ที่สามารถสั่งการมอเตอร์ให้หมุนตามมุม ความเร็วเชิงมุม ความยืดหยุ่นรอบจุด ค่าสัมประสิทธ์ความหน่วง และแรงบิดที่กำหนดได้ โดยมอเตอร์จะประเมินค่ามุม ความเร็วเชิงมุม และแรงบิดปัจจุบันเพื่อใช้ในการควบคุมได้ อย่างไรก็ตามเนื่องจากเวลาของการเชื่อมต่อไมโครคอนโทรลเลอร์กับอุปกรณ์มีค่าสูง จึงต้องเลือกใช้วิธีการเงื่อนไขทางเลือก (if-else) ร่วมกับสมการความยืดหยุ่นเสมือนต่อน้ำหนัก (IASPB) เป็นตัวจัดการแทนระบบ MLASCS ที่ใช้ปัญญาประดิษฐ์ หลังจากนั้น ตัวอย่างอุปกรณ์ชิ้นนี้ได้ถูกทำการวัดผล โดยมีการติดเซนเซอร์ไฟฟ้ากล้ามเนื้อ (EMG sensor) เพื่อใช้เป็นตัวชี้วัดคุณภาพของอุปกรณ์ โดยผลการทดลองสรุปได้ว่าอุปกรณ์ได้มีการช่วยเหลือการเดินเพียงบางครั้ง ในขณะที่บางครั้งมีการเพิ่มภาระให้กล้ามเนื้อแทน อย่างไรก็ดีลักษณะเช่นนี้อาจจะมีสาเหตุมาจากผู้ทดลองยังไม่เคยชินกับการใช้อุปกรณ์ การเดินไม่สมบูรณ์ในบางครั้ง หรือการส่งสัญญาณมีความล่าช้า ดังนั้นในอนาคต หากมีการทดลองเพิ่มเติมในแง่ของจำนวนผู้ทดลองและความเคยชินในการเดิน อาจจะทำให้เห็นชัดได้ว่าอุปกรณ์สามารถช่วยเหลือในการเดินได้หรือไม่

สาขาวิชา	วิศวกรรมเครื่องกล	ลายมือชื่อนิสิต ....
ปีการศึกษา	2565	ลายมือชื่อ อ.ที่ปรึกษาหลัก ....

6470007521 : MAJOR MECHANICAL ENGINEERING

KEYWORD: Knee Exoskeleton, Knee Reinforcement Device, Gait Rehabilitation, Machine Learning, Artificial Stiffness

Khemwutta Pornpipatsakul : Simulation and Prototyping of a Knee Assistive Device for Improved Gait Function. Advisor: NOPDANAI AJAVAKOM

This study aimed to develop a knee-assistive device while walking. The research was separated into two sections: the gait support simulation in MATLAB and the prototype of the device. Data on body part positions and ground reaction force were collected from three adult Thai participants walking at a speed of 1.5 m/s to calculate knee moment. The simulation section provides support moments during walking using machine learning and artificial stiffness control strategy (MLASCS), composed of the kNN model and the instantaneous artificial stiffness per body mass (IASPB) equations. The MLASCS was used to determine the proper amount of support moment required to assist walking, and its validation via the recorded data showed that it could reduce the total effort by up to 63.4%. In the prototype section, the posterior-support device was designed using a 3D printing filament and tested for durability. The control system used an actuator replicated from an MIT mini-cheetah servo motor that commanded various parameters such as angular, angular velocity, angular stiffness, angular damping coefficient, and angular moment and provided feedback in the form of angular angular velocity and angular moment. Due to a significant increase in delay time when connecting the microcontroller to the device, the sets of the if-else function called a state classifier combined with the IASPB equations were selected as the control system instead of the MLASCS. Efficiency testing was conducted using electromyography (EMG) sensors, which revealed mixed results that the device was sometimes helpful and sometimes not helpful. These may be due to an imperfect gait cycle, motor command delays, and misalignment of the device, indicating that further data collection and validation with more samples is necessary to verify the device's usefulness.

Field of Study:	Mechanical Engineering	Student's Signature ....
Academic Year:	2022	Advisor's Signature ....

ACKNOWLEDGEMENTS

I would like to express my sincerest gratitude to Assoc. Prof. Nopdanai Ajavakom, Ph.D., from the Department of Mechanical Engineering, Faculty of Engineering, Chulalongkorn University, for his invaluable guidance, unwavering support, and tireless effort in supervising my thesis. His expertise and insights were instrumental in shaping the direction of my research.

I would also like to extend my heartfelt thanks to Asst. Prof. Ronnapee Chaichaowarat, Ph.D., from Chula International School of Engineering, for his continuous encouragement, fruitful discussions, and generous provision of facilities in his laboratory, which greatly contributed to the success of my project.

Furthermore, I am deeply grateful to Miss Akkaraya Silsungvorn and Mr. Supawit Ittinirundorn, staff of the Faculty of Sport Science, for their kind assistance and provision of necessary facilities for my research experiment. Their support was essential in enabling me to conduct the experiments smoothly.

Once again, thank you to all those who have helped me throughout this journey.

Khemwutta Pornpipatsakul

TABLE OF CONTENTS

Page

LIST OF TABLES

Page

LIST OF FIGURES

Page

Chapter 1: Introduction

An excessive amount of standing, sitting, running, and walking might result in physical aches, especially knee discomfort. Because the knees support the entire upper body weight during most human activities, it is fairly prevalent. People's daily life will be greatly impacted by knee pain, such as difficulty sitting, running, or walking, or a lack of confidence performing simple tasks [1]. As a result of the spinal cord, severe injuries, and other diseases, many patients also experience knee impairments like muscle weakness, discomfort, and paralysis [2, 3].

Several knee gadgets have been developed to treat knee issues. In general, knee reinforcement devices are mechanical or electromechanical. It's important to note that the knee reinforcement device's main objective is to lower or enhance the user's metabolism depending on the work [4]. The equipment should be comfortable and stable when worn by the user [5].

The support pattern of currently available knee devices can be categorized into four sides, according to earlier investigations by Zhang et al. [6]: lateral-support layout (outside), two-side support, improved-lateral support, and anterior/posterior support. There is about 38% outside lateral support [7-29]. About 10% of devices are two-sided supports [3, 30-34], 40% are improved lateral supports [35-55], and the other devices are anterior/posterior supports [6]. The most important aspect that needs to be taken into consideration is how the device's mechanism flexes and extends the knee in accordance with knee movement [6]. The knee joint is suggested to be described as a four-bar linkage mechanism in a study publication with a maximum center of rotation error when walking of 1.08 mm [56]. Also, the knee angle may not exceed 70 degrees during a typical gait cycle [57], therefore there may not be much of a shift in the center of rotation's position. Then, it can be considered that the upper leg and lower leg can instantly flex or extend around the fixed revolute joint.

Zhang et al also presented that Many studies of knee assistive devices use various different actuation types [6]: 1. The active actuation using an electric or pneumatic actuator as a power source, 2. The passive actuation device using power from the potential energy of the device structure, 3. The quasi-active actuation generating power from combining active and passive actuator. Approximately 73% of the study uses active actuation [3, 7-23, 30, 35-39, 41-47, 55, 58-67], 10% uses quasi-active actuation [24-26, 48-51, 54], and 17% uses passive actuation [27-29, 31-34, 52, 53, 68, 69]. Additionally, pneumatic artificial muscles (PAM) [3, 47, 55, 70], series elastic actuators (SEA) [40, 54, 58, 71, 72], motors [45, 46, 61, 67], and regenerative magnetorheological actuators (RMRA) [73, 74] were typically used in previous gait rehabilitation and human performance augmentation applications [75].

Due to the wearer's physical connection to the device, control mechanisms are required for all actuation types while developing knee exoskeletons. In order to ensure the wearer's security and comfort, the assistive moment can be produced in accordance with their motions and intentions. Various control methods for knee exoskeletons have been proposed, including assist-as-needed control, position-based trajectory tracking control, and bioelectric signal-based control. [75]. The previous research employed the following control techniques: 1. Hybrid position/force control by applying the rotary and linear encoder [47] and a gauge pressure sensor [55] to generate the support moment; 2. Using the force control [71, 72], the device is subjected to controlled force or torque; 3. Bounded control, which raises safety and avoids actuator saturation [45, 46]; 4. Impedance control, which maps the desired trajectory and stiffness [40, 58, 61, 67]; 5. position control [54, 73, 74], which monitors typical gait patterns and operate the device; 6. on-off control [70] which generates and degenerates support in a particular circumstance. 6. bioelectric signals-based control [3] that integrates the relationship between muscle activity and human movement.

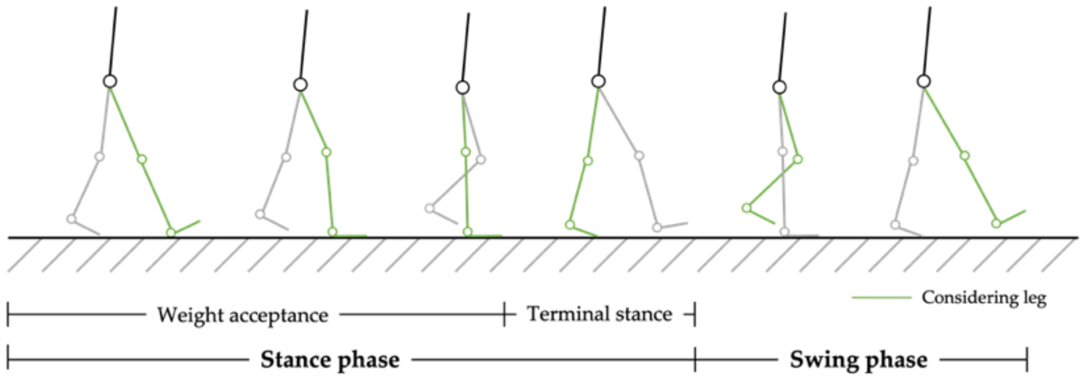

Figure 1 Human gait cycle (modified from [75, 76])

The knee angle, an angle between the thigh leg and shin leg where it is zero when two sections are parallel, is between 0 to around 70 degrees while walking, so the device should smoothly move between these degrees. The quadriceps muscles work across the knee joint as a pivot joint between the thigh and shin legs [77]. The knee joint's muscles, tendons, and ligaments can control the joint dynamic and static stability [78]. In addition, the joint can be assumed as a four-bar linkage [1, 56, 79] with a moving center of rotation point. The joint is stable because muscles and ligaments [2, 3] act as a damper. There are two basic phases in a normal human gait cycle: stance phase and swing phase, with the stance phase being further divided into the weight acceptance phase and terminal stance phase [75], as shown in Figure 1 (modified from [75]). The weight acceptance phase occurs when a foot begins to lie on the ground and sends body weight to the ground for balance. This phase ends when the foot fully presses the ground. The terminal stance phase starts when the foot begins to kick the ground to continue walking. The swing phase occurs after the foot has been propelled off the ground. It is the phase in which a foot does not touch the ground and swings to prepare for the next weight acceptance phase. Figure 2 shows the plots of human knee joint angle and moment per body mass during a gait cycle from modified raw data [57]. The maximum knee moment per body mass is around 0.67 Nm/kg. Note that the flexion moment is negative.

A possibility of whether the stance and swing phase can be predicted by the angular velocity of the lower leg was presented by Grimmer et al [80]. Attaching five inertial measurement units (IMUs) makes it possible to detect the stance phase while applying additional rule sets. The relative velocity between a thigh and shin leg was also suggested by Javanfar et al [81]. The relative motion between the femur and tibia can be analyzed by the collision reactions of the knee’s cartilage and bone. The results can suggest a design concept for a knee device.

The machine learning technique has been used for improving a knee device. Mokri et al [82] can estimate a muscle force from the prediction of several machine learning while the input is data from surface electromyography (sEMG) signals. This method can improve the performance of therapy and increase the sensitivity between the muscle model and the tendon stiffness. Machine learning was also applied for helping people with leg-missing disabilities [83]. The study showed that the data from a series of foot pressure sensors can be used to predict the walking phase through the k-nearest neighbor (kNN) algorithm. Not only healthy gait can be detected by a machine learning model, but an abnormal gait can also be predicted. Chen et al. presented that their algorithm can predict the probability of elderly flat ground which is helpful for rehabilitation monitoring [84].

The control techniques usually require many sensors to control knee devices because of the complexity of movement that the knee flexes and extends when the foot touches and does not touch the ground. Nowadays, actuators combined with an encoder can give feedback on the motor's current angle and the angular velocity of the joint. For reducing the number of sensors in the device, this research proposes Machine Learning and Artificial Stiffness Control Strategy (MLASCS) by using the knee angle and the knee angular velocity with machine learning and artificial stiffness techniques for controlling the amount of supporting moment of the knee assistive device in a gait cycle. The machine learning model is introduced to classify the state of a gait cycle for mapping the amount of stiffness to support the required knee moment. This study explains how to create the MLASCS and validates the efficiency of this strategy by simulating the effort used when walking with and without MLASCS. The results of this study can tell if machine learning can be applied to finding a state of gait, and amount of supporting knee moment. In addition, the study also designs the knee device with easy putting on and taking off, flexibility for fitting leg shape, and lightweight criteria for supporting gait, and verify the built device to see if the MLASCS can be used for knee devices. If not, the classifier for predicting the state of a gait cycle to control the device needs to be mentioned.

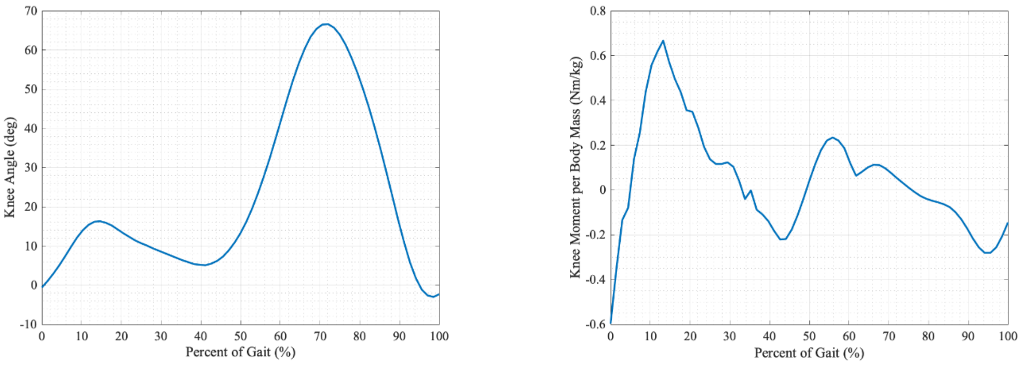

(a) (b)

Figure 2 Human knee joint angle (a) and moment per body mass (b) in a gait cycle.

The paper is organized as follows. Section 2 describes how to collect and prepare data for calculations. Section 3 gives details on the creation of the MLASCS composed of machine learning and artificial stiffness control techniques. In section 4, the simulation and validation of the MLASCS are shown. The results and discussion are displayed in Section 5. Finally, Section 6 concludes all details of the study and discusses future work.

Chapter 2: Knee Joint Data Collection of Walking Gait Cycle

Even though there is a lot of recorded knee joint data on a normal human gait cycle, there might not be much knee data measured on Asian people which differs from Western people. Therefore, the data in walking gaits are measured in our research laboratory to make sure the number of data points is enough for creating a machine learning model.

Chapter 2.1: Data Collection

To analyze and design an assistive knee motion device, knee angle and moment data are required which can be obtained through inverse kinematics calculations using ground reaction force (GRF). Motion capture and force plate sensors are effective in determining knee movement and GRF. Proper marker placement is necessary for accurate measurement, and according to recommendations by Robertson et al. [85], at least two positions in each segment should be marked. To this end, markers were attached at the CG, hip, knee, ankle, and fingers as shown in Figure 3. The average walking speed of all participants was 1.5 m/s.

The CG marker, placed around 0.412 of sample height (proximal) following Robertson et al.'s recommendation [85], was used to estimate walking speed. Other markers, including the hip, knee, ankle, and finger markers, were attached according to the Qualisys Software Manual for 3D position measurement to calculate knee and ankle angles. The experiment involved three Thai adult participants with an average age of 23, a height of 171-172 cm, and a weight of 51.9-61.8 kg. The measurements were taken using two force plate sensors on the ground and sixteen marker detectors, one camera, and a marker position setup as shown in Figure 4. Nine trials were conducted in total.

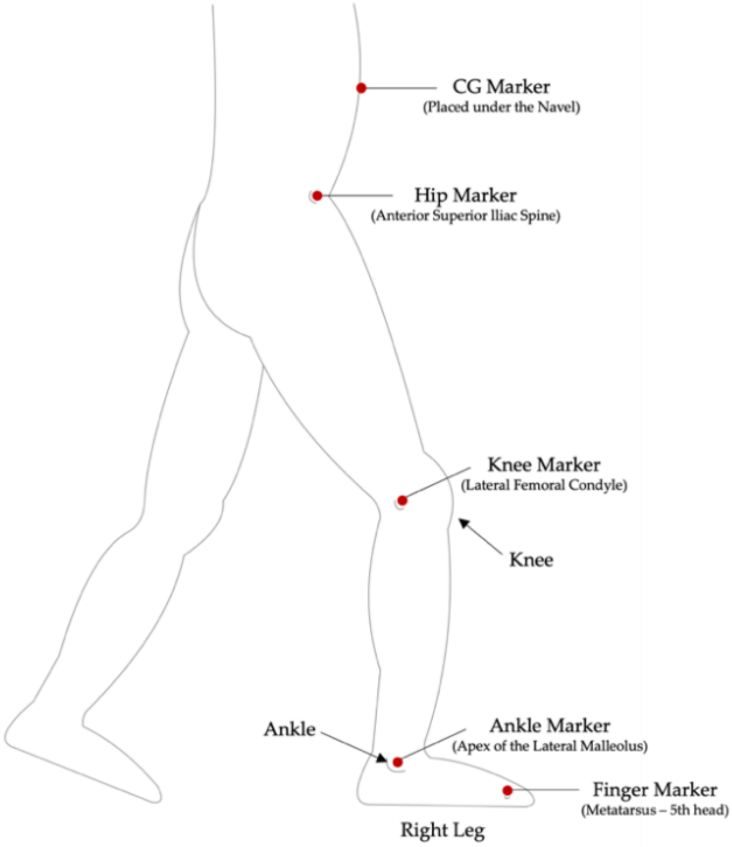

Figure 3 Positions of markers for collecting data from the Qualisys motion capture system.

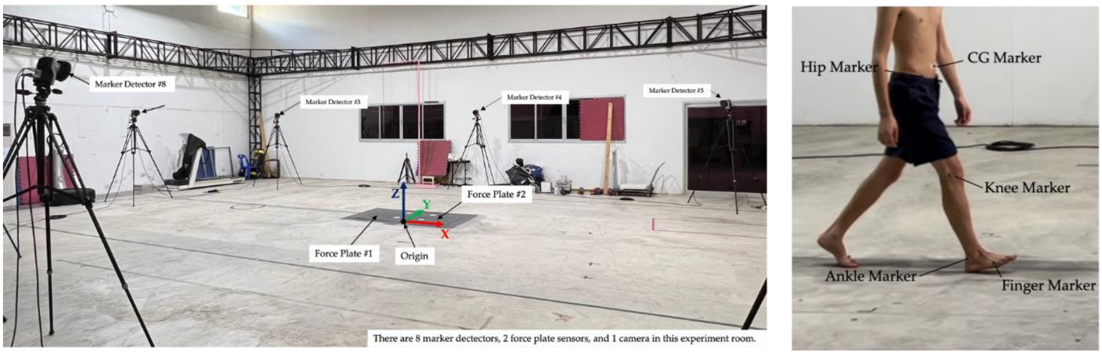

(a) (b)

Figure 4 The experiment room consists of 8 marker detectors, 2 force plates, and 1 camera and the origin and axis of the tests (a), and the position of the marker on the participant (b).

Chapter 2.2: Data Analyzing

The recorded data from the motion capture was resampled to have a uniform sampling frequency of around 240 Hz using MATLAB. Additionally, MATLAB was used to remove any noise present in the data.

Kinematics of Knee

The raw 3D position data of the CG, hip, knee, ankle, and finger markers were used to determine the knee and ankle angles. Since the variation in the y-axis data is negligible, only the X-Z plane data was analyzed. To perform further calculations, velocity and acceleration needed to be calculated from the position and angle data. The Centered Finite-Difference (CFD) method with an accuracy of order four was utilized for this purpose. The regular CFD equation [86]:

$$f'(x)=\frac{[f(x+h)-f(x-h)]}{2h} \tag{1}$$

can be calculated for more accurate prediction in the first derivatives for velocity [87]

$$f'(x)=\frac{[-f(x+2h)+8f(x+h)-8f(x-h)+f(x-2h)]}{12h} \tag{2}$$

and second derivatives for acceleration [87]

$$f''(x)=\frac{[-f(x+2h)+16f(x+h)-30f(x)+16f(x-h)-f(x-2h)]}{12h^2} \tag{3}$$

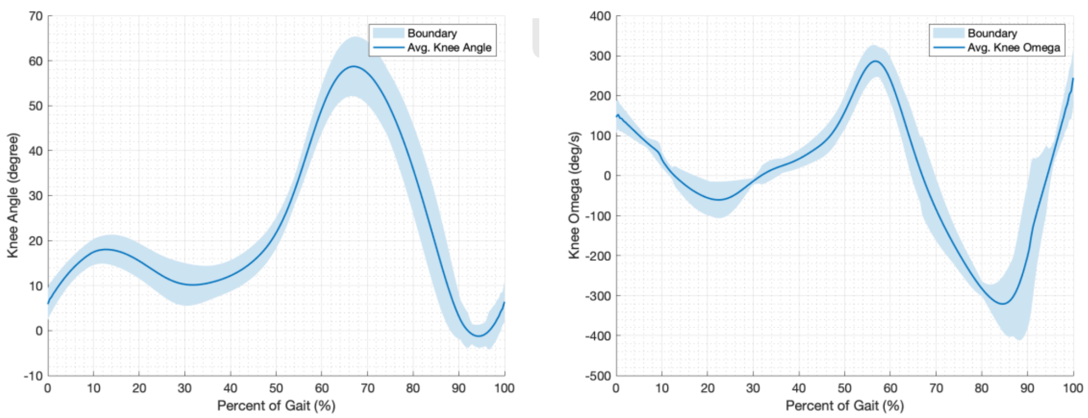

(a) (b)

Figure 5 The average and the boundary of the maximum and minimum of all post-processed data in (a) The knee angle; (b) The knee angular velocity (knee omega).

where x is the time values, f(x) is the function, f'(x) is the first derivative function, f''(x) is the second derivative function, and h represents the small step time.

Based on the collected data, some noise was observed in the knee angle data, which required post-processing signal filtering before determining the knee angular velocity (knee omega) and CG velocity for convincing the speed of walking where the plot of CG speed is shown in figure A.1 in Appendix A.. Figure 5 shows the average of the processed knee angles and knee omegas with the boundaries of all nine-trial data, with the starting position being when the heel touches the force plate. The average data for knee and ankle angles, angular velocity, and angular acceleration of all trials are presented in Table B.1 in Appendix B.

Kinetics of Knee

The following is the process for calculating knee moment (M_{knee}) from the GRF. All equations are modified from Newton's 3rd Law (equations 4-5) for planar motion where the free body diagrams of the lower leg and the foot are shown in Figure 6. There are two steps in this calculation. The first step is the calculation of both x and z directions of the ankle reaction force ($F_{x,\ ankle}$ and $F_{z,\ ankle}$) and the ankle moment (M_{ankle}) from the x and the z directions of the GRF (GRF_x and GRF_z) shown in equations 6–8,

$$\sum F = ma, \tag{4}$$

$$\sum M_G = I\alpha \tag{5}$$

where $\sum F$ represents the summation of all the forces that act on the body, m is the mass of the body, and a is the acceleration of the body. $\sum M$ is the summation of all action moments exerted on the body around a specific point (G), the I is the moment of inertia of the body around the point, and the α is the angular acceleration of the body around the point. From the free body diagram of the lower leg and foot shown in figure 6, the forces on the ankles are:

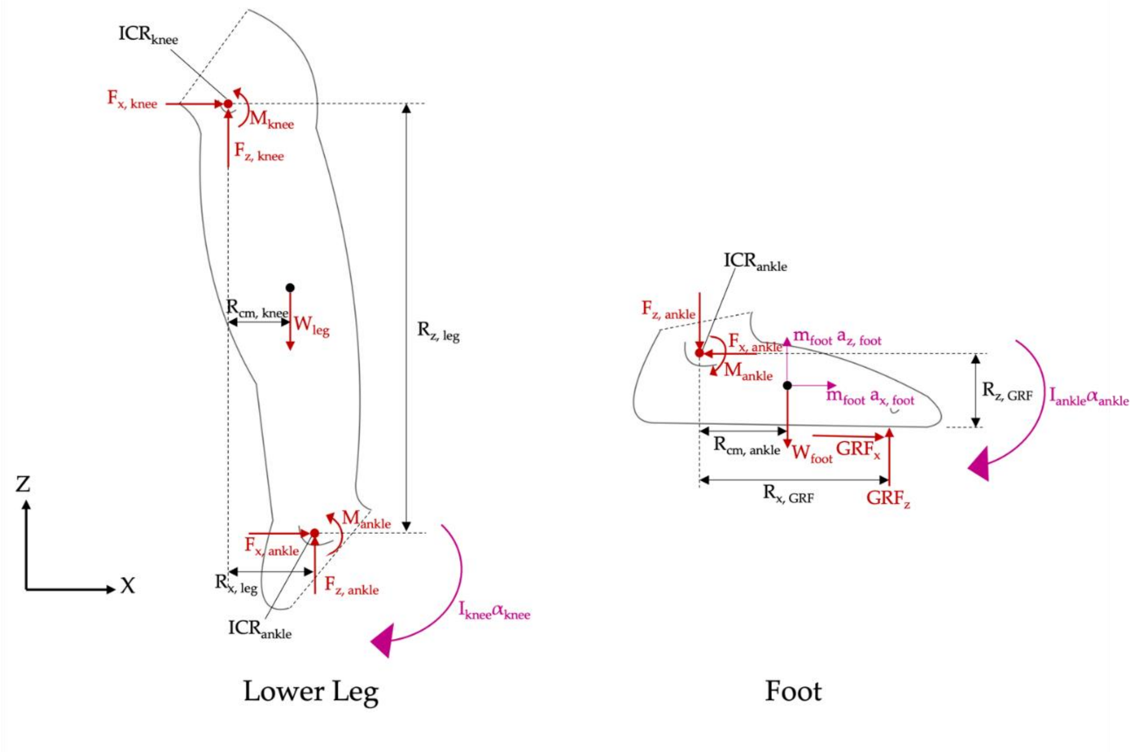

Figure 6 The free body diagrams of the lower leg and the foot for calculating the knee moment.

$$F_{x,ankle}=GRF_x-m_{foot}a_{x,foot} \tag{6}$$

$$F_{z,ankle}=GRF_z-W_{foot}-m_{foot}a_{z,foot} \tag{7}$$

And the moment around the ankle is

$$M_{ankle}=GRF_z\left(R_{x,GRF}\right)+GRF_x\left(R_{z,GRF}\right)-W_{foot}\left(R_{cm,ankle}\right)+I_{ankle}\alpha_{ankle} \tag{8}$$

where the GRF_x and GRF_z are the ground reaction force in the x and z directions, respectively, shown in Figure 7. The $R_{x,\,GRF}$ and $R_{z,\,GRF}$ are the lever arm distance between the instantaneous center of rotation of the ankle (ICR_{ankle}) and GRF_x and GRF_z, respectively. Note that, the position data of the ankle marker, placed at the apex of the lateral malleolus, was used as the position of the ICR_{ankle} in this calculation. The mass m_{foot} is the estimated mass of the foot, which is approximately 0.0145 of body mass (m_{body}) [85], $a_{x,\,foot}$ and $a_{z,\,foot}$ are the accelerations at the foot's center of mass in the x and z-directions, W_{foot} is the weight of the foot.

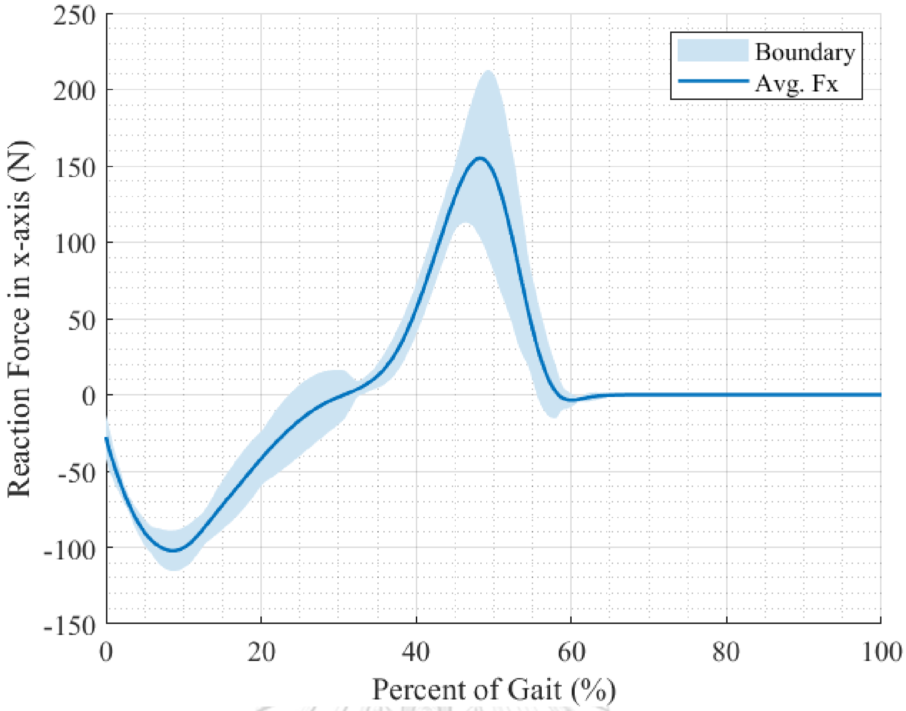

(a)

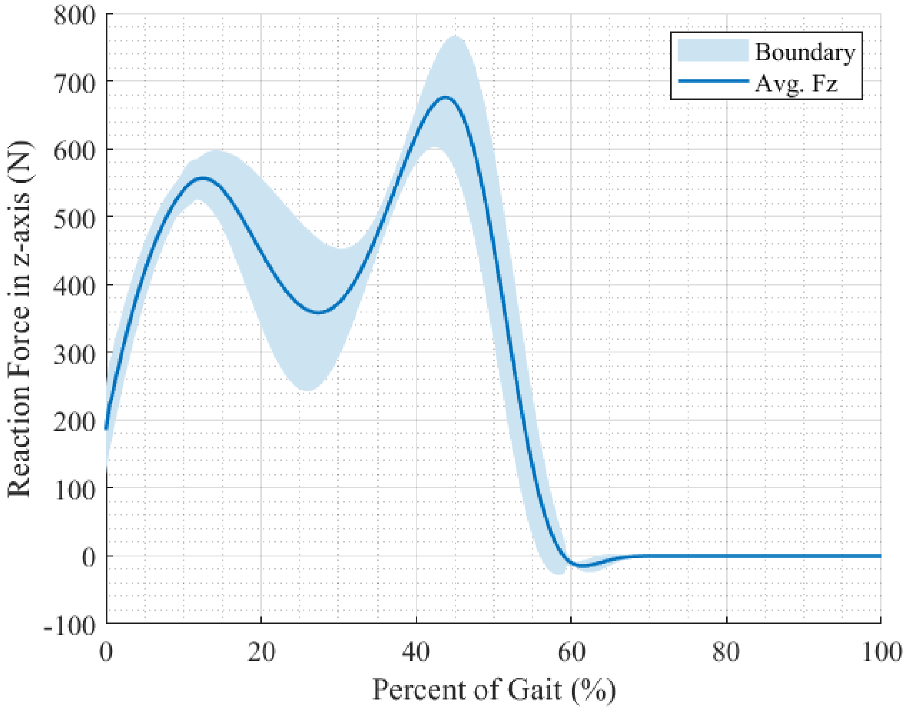

(b)

Figure 7 The average and the boundary of Ground reaction force (GRF) in x and z axis

The $R_{cm,\ ankle}$ is the lever arm distance between the ICR_{ankle} and W_{foot}, I_{ankle} is the moment of inertia around ICR_{ankle} of which the radius of gyration is approximately 0.690 of the foot length [85], and α_{ankle} is the angular acceleration of the ankle. All positions of the variables are shown in Figure 6, where $F_{x,\ knee}$ and $F_{z,\ knee}$ are the knee reaction forces in the x and z direction, respectively. Hence, the moment of the knee M_{knee} can be calculated from $F_{x,\ ankle}$, $F_{z,\ ankle}$ and M_{ankle} via equation:

$$M_{knee}=W_{leg}\left(R_{cm,knee}\right)-M_{ankle}-F_{z,\ ankle}\left(R_{x,\ leg}\right)-F_{x,\ ankle}\left(R_{z,\ leg}\right)+I_{knee}\alpha_{knee} \tag{9}$$

where W_{leg} is the weight of the lower leg which is approximately 0.0465 of body mass [85], $R_{cm,\ knee}$ is the level arm distance between the instantaneous center of rotation of the knee ICR_{knee} and W_{leg}, $R_{x,\ leg,}$ and $R_{z,\ leg}$ are the lever arm distances between ICR_{knee} and $F_{x,\ ankle}$ and $F_{z,\ ankle}$, respectively, I_{knee} is the moment of inertia around ICR_{knee} of which the radius of gyration is approximately 0.528 of the lower leg length [85], and α_{knee} is the angular acceleration of the knee. The average reaction force of the ankle, and moment around ankle and knee of all trials are shown in table B.2.

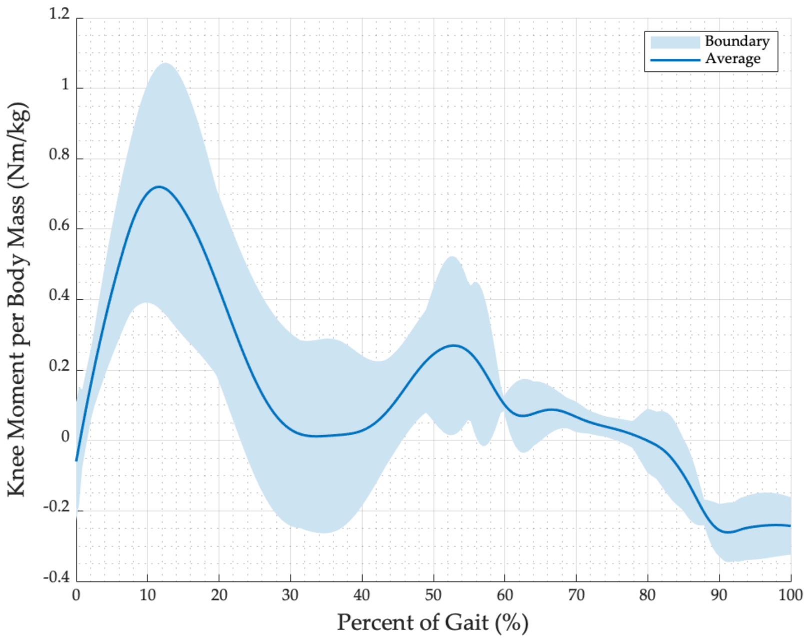

Figure 8 The average and the boundary of the knee moment per body mass from the calculations.

The knee moment per body mass (MPB_{knee}) during a gait cycle of all trials can be determined from the knee moment (M_{knee}) and the body mass (m_{body}):

$$MPB_{knee}=\frac{M_{knee}}{m_{body}}. \tag{10}$$

The average and boundary values of knee moment per body mass are presented in Figure 8, where positive values indicate knee extension moment and negative values indicate knee flexion moment. Although the results differ slightly from Winter's [57] previous study, the overall trends of knee moments are similar. Differences in step lengths, foot shapes, stride patterns, and other factors may account for the variations in the results. Moreover, knee moment paths may differ even within the same person across steps. Therefore, it is reasonable to observe variations in knee moments among different individuals.

Chapter 3: Simulation in MATLAB

A critical step in the development of a knee assistive device is the validation and testing of the control system. To ensure the safety and efficacy of the device, it is advisable to validate the control system through simulation before deployment. In this regard, we present a simulation study comprising three parts: 1) Machine Learning and Artificial Stiffness Control Strategy (MLASCS), the control system utilized for simulation, 2) Simulation and Validation, and 3) Results and Discussions. The simulation results will provide insight into the effectiveness of the control strategy and its ability to support high knee moments during walking. The findings from this study will aid in the development of a safe and efficient knee assistive device for those in need.

Chapter 3.1: Machine Learning and Artificial Stiffness Control Strategy (MLASCS)

The Machine Learning and Artificial Stiffness Control Strategy (MLASCS) is proposed as a promising approach to control a knee assistive device in a gait cycle. Unlike traditional methods that rely on a wide range of information, only the knee angle and angular velocity (knee omega) are required to determine the state of a gait cycle and the amount of support moment provided by the device. To ensure the safety of the wearer, the MLASCS control system should be combined with a possibility checking function, which can increase the accuracy of state prediction, and various stiffness functions that can enhance the suitability of supporting moment. Additionally, the use of artificial stiffness with a goal position can generate a moment of direct command. Artificial stiffness is a function that can predict the amount of stiffness required to support gait based on the knee angle and the state of gait.

Classification and Training for Machine Learning Model

In order to determine the appropriate knee moment support at any position of a gait cycle, it is necessary to classify the walking stage, which consists of two main phases: the stance phase and the swing phase. However, a single knee angle can occur in both phases. Thus, it is essential to develop a machine learning model that can accurately classify the walking state and predict the phase to provide proper knee moment support.

Classification

It has been previously established that a single knee angle cannot be used to determine the position of a gait cycle or the state of walking. Therefore, knee omega is proposed as the second variable for classifying the state. Figure 9 displays the post-processed knee angle and knee omega data for all nine-trial data, and their relationship. However, it should be noted that the inner and outer loop cannot be directly mapped to the swing and stance phases. Thus, a new set of states should be defined to allow for more precise control in this system.

Based on the observations from a gait cycle, a classification of four states can be made by identifying the local minimum and maximum points in a knee angle. These states are named as Initial Place, Final Place, Initial Lift, and Final Lift states, with each state's position shown in Figure 9. The mapping of these states to a gait cycle is illustrated in Figure 10. The Initial Place state is marked by a fully extended knee before the heel touches the ground (Omega is more than zero within the inner loop). After the knee extends due to body weight while being placed on the ground, the Final Place state starts (Omega is less than zero within the inner loop). The Initial Lift state starts when the foot kicks the ground and starts flexing within the stance phase (Omega is more than zero). Finally, the Final Lift state occurs when the knee extends for a heel strike in the next gait cycle (Omega is less than zero). By using these four states, a machine learning model can be trained to classify the walking stage and determine proper knee moment support at any position of a gait cycle.

Based on the observation of the gait cycle, the knee angle in the Initial and Final Place states does not exceed 25 degrees. In the Initial Place state, the knee omega is positive while it is negative for the Final Place state. For the Initial and Final Lift states, the knee omegas have the same characteristics as the Initial and Final Place states, but the knee angle can be up to 70 degrees based on the recorded data.

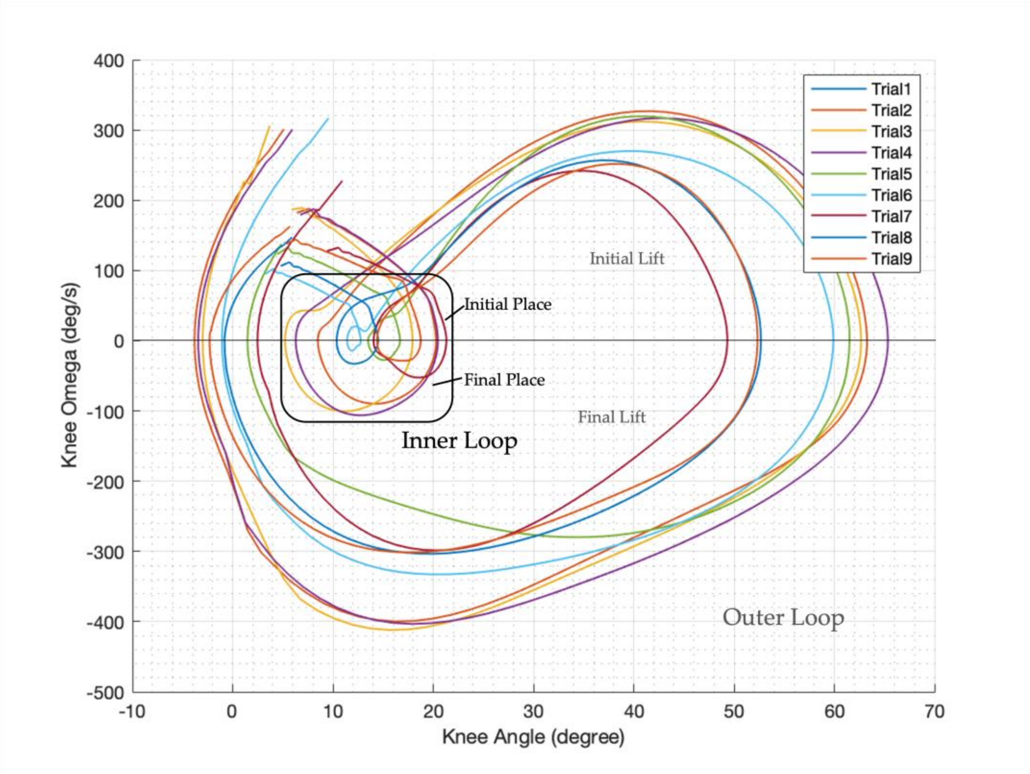

Figure 9 The plot of the nine-trial recorded Knee Angle from post-processed recorded data and Knee Omega from post-processed and calculated recorded data by equation 2 which the plot can be separated into Initial Place, Final Place, Initial Lift, and Final Lift states.

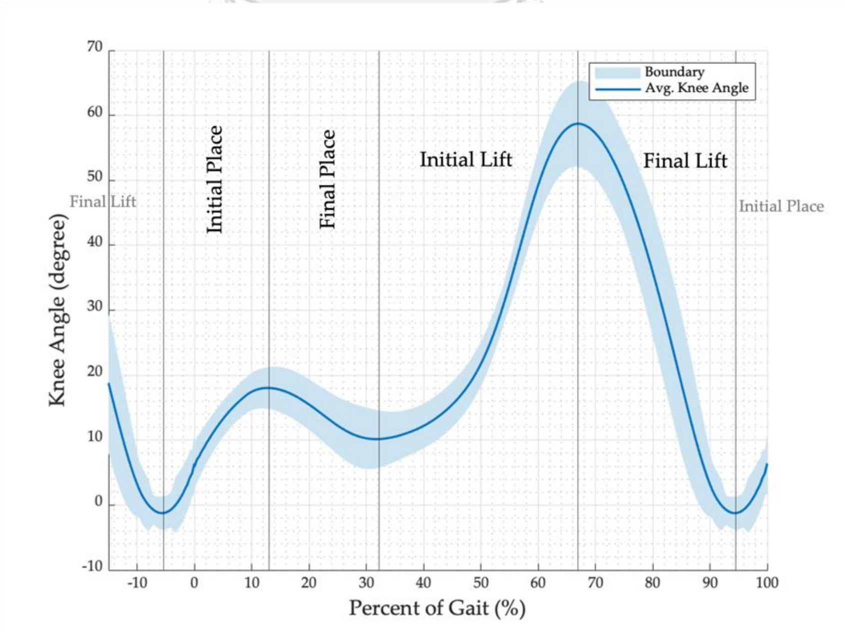

Figure 10 Knee angle and states of a gait cycle.

Training

After defining the states of all training data, MATLAB version R2022b (MathWorks, Natick, MA, USA) was used for data analysis. The Statistics and Machine Learning Toolbox was used for classification. The advantage of using a machine learning technique is its ability to classify accurately even with a large amount of training data. It is important to note that the model should be able to predict the state correctly for a specific gait speed before testing with different gait speed training data. This study focuses on a gait speed of approximately 1.5 m/s. The training data was tested with several classifiers including decision trees (accuracy: 80.0%-92.5%), discriminant analysis (accuracy: 76.6%-77.1%), Naïve Bayes classifiers (accuracy: 77.6%-81.5%), support vector machines (accuracy: 84.8%-93.7%), and nearest neighbor classifiers (accuracy: 78.8%-95.0%). The K-Nearest Neighbor (KNN) algorithm was found to be the most accurate classifier with an accuracy of approximately 95.0%. Table 1 shows the training settings for the KNN classifier.

Table 1 The settings for training the KNN machine learning model.

Setting	Detail
Preset	Fine KNN
Number of Neighbors	3
Distance Metric	Chebyshev
Distance Weight	Equal
Standardize Data	True

Improving

The Continuity of State Checking (CoSC) is a technique used to improve the prediction accuracy of the machine learning model. It confirms the correctness of the prediction by checking the last and current predicted states. Since walking is a continuous loop posture, the CoSC ensures that the predicted state always follows the loop of states in a gait cycle.

By applying the CoSC to the machine learning model, the accuracy has increased to 99.9%, as seen in the validation Confusion Matrix in Figure 11. The number of the test data is 1260. One data was predicted as the final place state instead of the initial place state, and one data was predicted as the initial place state instead of the final lift state. However, the accuracy of the model may decrease if it is used to predict data from gait speeds other than 1.5 m/s, since the model was trained on data from that specific gait speed.

One limitation of the machine learning model is its processing time. The fastest prediction speed is around 168 observations per second, and this speed may vary depending on the computer and its processor.

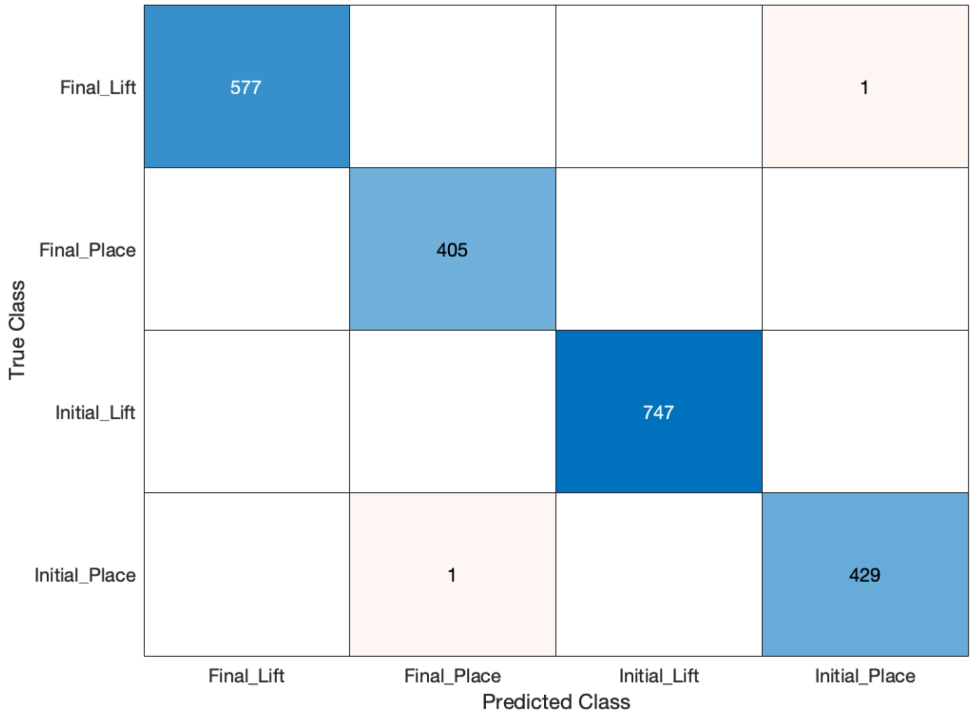

Figure 11 The Validation Confusion Matrix of the machine learning model by testing from 1,260 test data. One data was predicted as the final place state instead of the initial place state, and one data was predicted as the initial place state instead of the final lift state.

Artificial Stiffness Control

An artificial stiffness control mechanism represents a promising approach to support knee moments during the gait cycle. This approach was inspired by the observation of a torsion spring's ability to generate a return moment when it moves from rest. By commanding a controllable actuator with the desired position, the artificial rest position, and the proportional gain, it can emulate a torsion spring with the desired stiffness. In comparison to the direct torque applied method, this technique may be more user-friendly, as the supporting moment acts like an elastic spring. As the actuator approaches the desired position, the generated moment should decrease and eventually come to a stop upon reaching the desired position.

Instantaneous Artificial Stiffness (IAS)

The estimation of instantaneous artificial stiffness (IAS) involves determining a constant angle deflection value that is added to the knee angle, and using this value along with the knee moment (M_{knee}) to calculate the IAS. A low deflection angle value results in a higher IAS, while a high deflection angle value results in a lower IAS. This relationship can be seen in the equation used to calculate knee moment.

$$M_{knee} = \text{IAS x (deflection angle)}, \tag{11}$$

Therefore, in this study, a deflection angle of 10 degrees was chosen since the instantaneous artificial stiffness was not too high, and it provided sufficient deflection for actuator operation. To estimate the instantaneous artificial stiffness per body mass (IASPB), the MPB_{knee} was utilized instead of the M_{knee}, as shown in Equation 12, where 'i' represents the knee angle in degrees:

$$\text{IASPB}(i)=\frac{MPB_{knee}(i)}{10} \tag{12}$$

Artificial Stiffness Control Equations

In order to make the estimation of instantaneous artificial stiffness per body mass (IASPB) applicable to different individuals with varying gait cycles, equations were derived to estimate the IASPB throughout a gait cycle. The average knee moment per body mass ($AMPB_{knee}$) was obtained by averaging all MPB_{knee} values and was used to derive IASPB equations for each state using the polyfit function in MATLAB. Equations 13-16 show the $IASPB_{IP}$, $IASPB_{FP}$, $IASPB_{IL}$, and $IASPB_{FL}$ functions, which represent the IASPB in the Initial Place, Final Place, Initial Lift, and Final Lift state, respectively, where "a" is the knee angle. The plots of the IASPB path on the knee angle in all trials and the estimated values from the equations in each state are presented in Figure 12. The equations of IASPB in the initial and final place, and final lift can be mapped into the second-degree polynomial equations, but the initial place required the fifth-degree equation due to the complexity of the plot. The positive values indicate the extension direction, while the negative values indicate the flexion direction.

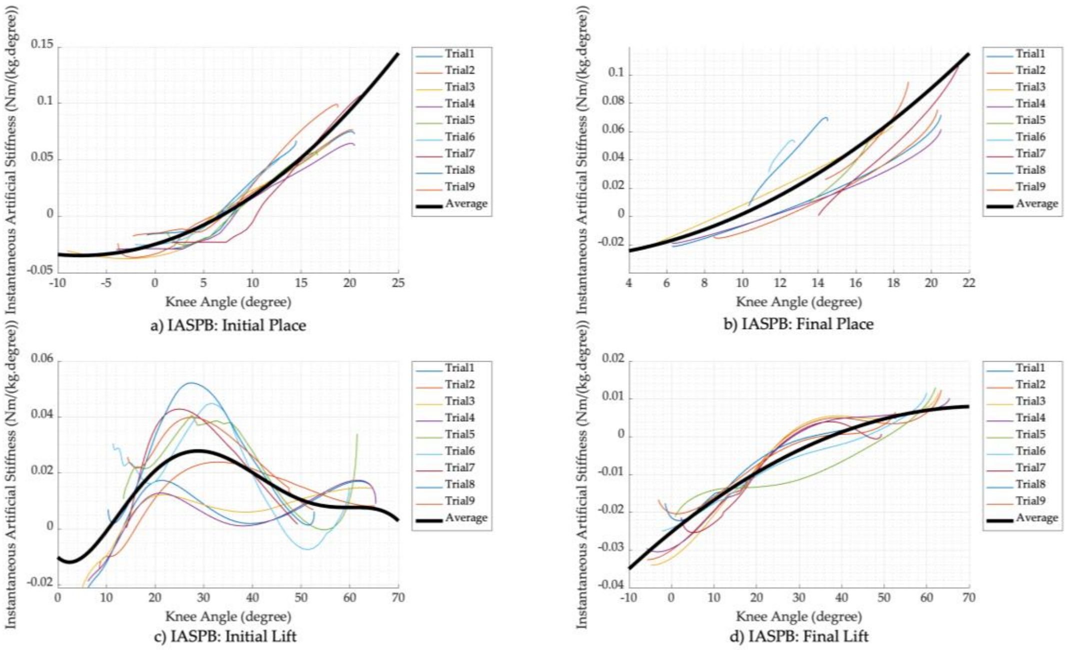

Figure 12 The Instantaneous Artificial Stiffness per body mass (IASPB) path on the knee angle in (a) The Initial Place state; (b) The Final Place state; (c) The Initial Lift state; (d) The Final Lift state.

The proposed system integrates Artificial Stiffness Control with machine learning, as illustrated in Figure 13. The machine learning model utilizes the current knee angle (θ) and angular velocity (ω) measured by the encoder to predict the current state of the gait cycle. Based on the predicted state and θ, the current IASPB is calculated. Multiplying the IASPB by the body mass results in an Instantaneous Artificial Stiffness (IAS) value. To generate the supporting moment for the knee, the actuator requires both the IAS and the desired position ($\theta_{desired}$), which is set to be 10 degrees away from θ. Finally, the IAS and $\theta_{desired}$ are utilized to command the actuator.

$$IASPB_{IP}\,(a) = 0.0073a^2 + 0.0391a + 0.0179 \quad (13)$$

$$IASPB_{FP}\,(a) = 0.0023a^2 + 0.0237a + 0.0303 \quad (14)$$

$$IASPB_{IL}\,(a) = -0.002a^5 + 0.0057a^4 + 0.0067a^3 - 0.026a^2 + 0.0019a + 0.0279 \quad (15)$$

$$IASPB_{FL}\,(a) = -\,0.0028a^2 + 0.0111a - 0.003 \quad (16)$$

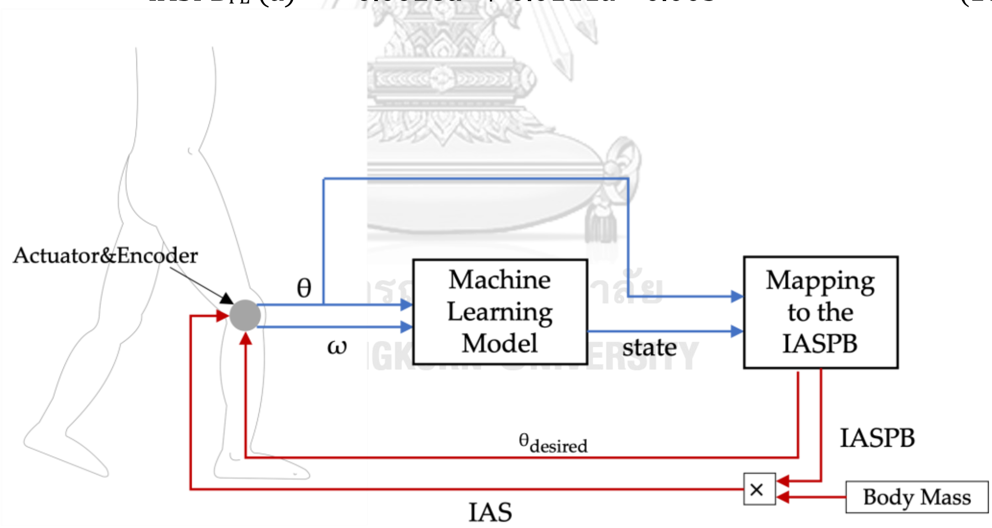

Figure 13 The concept of Artificial Stiffness Control combined with machine learning.

Chapter 3.2: Simulation and Validation

This section describes the simulation method used to validate the MLASCS concept and compare the walking efficiency over a gait cycle, with modifications based on [31]. The simulation utilized the average knee angle and knee omega data from all nine-trial recordings for testing. The supporting moment, generated by the actuator to assist walking, was estimated using the instantaneous artificial stiffness (IAS) equations. The simulation followed the same path as shown in Figure 13, where the sample knee angle and omega predicted the gait state using the machine learning model. The predicted state and knee angle were then used to calculate the IASPB using equations 13-16. The IASPB was multiplied by the sample mass to predict the amount of supporting moment, which was then multiplied by the angle deflection to calculate the supporting moment. The validation was performed by comparing the effort required over a gait cycle with and without the supporting moment.

Supporting Moment Simulation

The simulation settings were done to have the test as close to the real system. The knee angle (θ) and the knee omega (ω) of the sample were imported one set at a time. Then, this set was used to predict the state and determine the IAS and $\theta_{desired}$. The IAS from the IASPB equations can be either positive or negative, but stiffness in negative has no meaning. In the case that the IAS is negative, it will be change to positive, and the $\theta_{desired}$ will be negative instead. The IAS, θ, and $\theta_{desired}$ can be used to estimate the supporting moment (M_s) with an adjustable percentage of support (n), between 0-1, by the following equation:

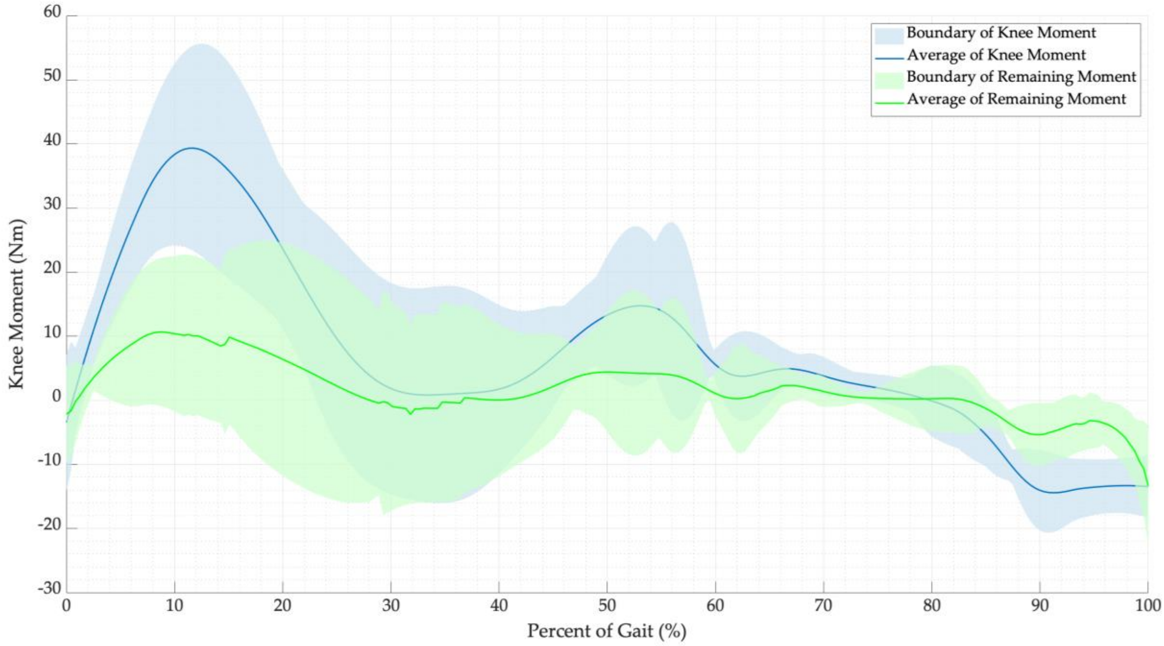

Figure 14 Plots of the average and boundary of knee moment (M_{knee}) and remaining knee moment (M_r), the moment that is still required for walking after being supported by the device when the percentage of support (n) is 0.7.

$$M_s = n|IAS|\,(\theta - \theta_{desired}), \tag{17}$$

and M_s was used to calculate the remaining knee moment (M_r), the moment that is still required for walking after being supported by the device, via the equation:

$$M_r = M_{knee} - M_s. \tag{18}$$

After simulating multiple sets of gait data, it was discovered that the generated supporting moment (M_s) was often higher than the required moment, which indicated over-assistance. To address this issue, the percentage of support was optimized to prevent such moments in all trial data. The percentage of support (n) was found to be less than 70% or 0.7. Subsequently, all M_{knee} values were compared to their average and boundary when n was set to 0.7. This comparison is illustrated in Figure 14.

Effort over a gait cycle

To validate and compare the MLASCS concept, an effort analysis over a gait cycle was conducted using the methodology presented by Chaichaowarat et al [31]. The effort over a gait cycle was divided into two components, the Extension Effort (EE) and Flexion Effort (FE), which were obtained by integrating the Extension Moment (EM) and Flexion Moment (FM) over a Percent of Gait (PoG) using Equations 19-20. The Total Effort (TE) was then calculated by summing the EE and FE using equation 21. This approach was used to quantify the difference in effort between the sample path and the resulting path obtained with assistance from the device. The efforts for each trial were calculated from the measured knee moment, while the remaining efforts were determined from the moments with assistance from the device. The resulting effort profiles are shown in Figure 15.

$$EE=\int_0^1 EM\, dPoG \tag{19}$$

$$FE=\int_0^1 FM\, dPoG \tag{20}$$

$$TE = EE + FE \tag{21}$$

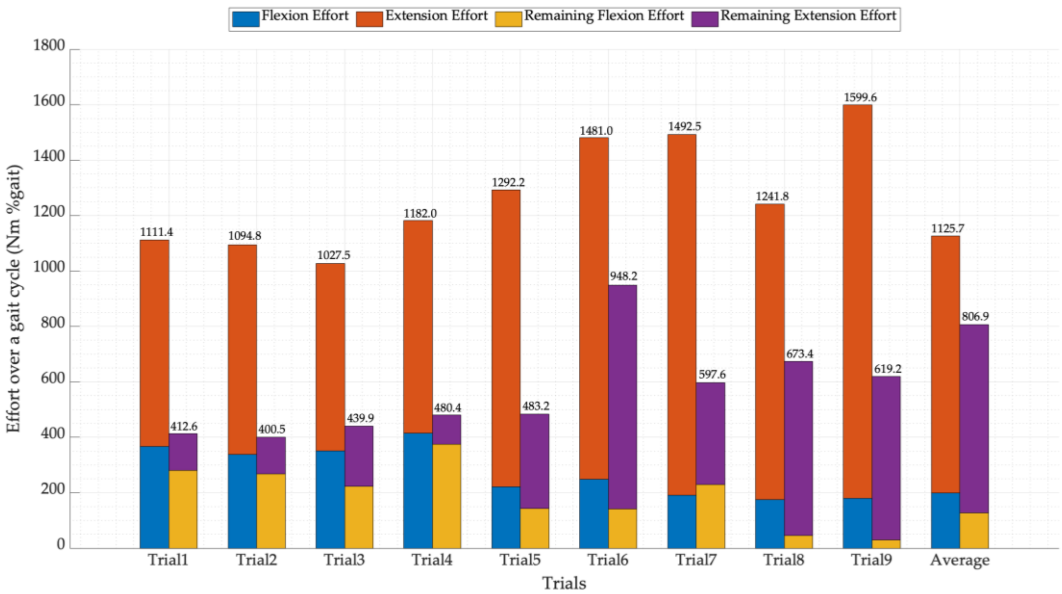

Figure 15 Comparison of the effort over a gait cycle from recording walking data and remaining effort over a gait cycle in each trial. Note that the numbers shown at the top of the bars are the total effort of each bar.

Chapter 3.3: Results and Discussion

Knee assistive devices rely on knee angle and knee moment data to ensure safe and effective device control. To optimize device control during walking gait, additional information regarding the gait phase is required, as varying levels of support are needed during different phases. To address this need, the Machine Learning and Artificial Stiffness Control Strategy (MLASCS) has been developed to classify the four phases of gait: initial place, final place, initial lift, and final lift. This classification is then used in conjunction with knee angle data to estimate the appropriate level of support required via the instantaneous artificial stiffness per body mass (IASPB) equations discussed in the previous section.

The IASPB equations, which calculate the instantaneous artificial stiffness per body mass, were divided into four functions: $IASPB_{IP}$, $IASPB_{FP}$, $IASPB_{IL}$, and $IASPB_{FL}$, each corresponding to the Initial Place, Final Place, Initial Lift, and Final Lift state, respectively. To ensure that the supporting moment generated does not exceed or fall short of the required knee moment for walking, each IASPB function was calculated using the average knee moment per body mass ($AMPB_{knee}$). A percentage of support (n) was introduced to adjust the supporting moment, with the optimal value of n being 0.7 to prevent over-assisting moments.

In the simulation section, the MLASCS was tested using both the recorded trial data and average data to validate the efficiency of the strategy. The effort over a gait cycle was used as a metric to compare the results obtained with and without assistance. The results indicate that the machine learning model's prediction accuracy is high, and the IASPB equations can provide the necessary stiffness to support the knee in each position, which is generally slightly lower than the required amount for walking. The total effort of the recorded data was normalized to 100% for easy comparison with the total effort after support was provided in each trial, as presented in Table 2.

Table 2 . Comparison of the Effort over a gait cycle from recorded data and Remaining Moment.

Trials	Data	Flexion Effort (FE)	Extension Effort (EE)	Total Effort (TE)	Reduction
Trial 1	Effort without Assist	33.0%	67.0%	100%	62.9%
	Remain Effort	25.2%	11.9%	37.1%	
Trial 2	Effort without Assist	30.9%	69.1%	100%	63.4%
	Remain Effort	24.4%	12.2%	36.6%	
Trial 3	Effort without Assist	34.2%	65.8%	100%	57.2%
	Remain Effort	21.8%	21.0%	42.8%	
Trial 4	Effort without Assist	35.1%	64.9%	100%	59.4%
	Remain Effort	31.7%	8.9%	40.6%	
Trial 5	Effort without Assist	17.1%	82.9%	100%	62.6%
	Remain Effort	11.0%	26.4%	37.4%	
Trial 6	Effort without Assist	16.8%	83.2%	100%	36%
	Remain Effort	9.6%	54.4%	64.0%	
Trial 7	Effort without Assist	12.8%	87.2%	100%	60%
	Remain Effort	15.3%	24.7%	40.0%	
Trial 8	Effort without Assist	14.1%	85.9%	100%	45.8%
	Remain Effort	3.6%	50.6%	54.2%	
Trial 9	Effort without Assist	11.3%	88.7%	100%	61.3%
	Remain Effort	1.8%	36.9%	38.7%	
Average	Effort without Assist	17.7%	82.3%	100%	28.3%
	Remain Effort	11.3%	60.3%	71.7%	

The analysis of the total effort of the remaining after supporting in each trial demonstrated that the MLASCS was effective in assisting knee moments during walking. The percentage of remaining effort was found to be dependent on the percentage of support (n) selected for the individual user. If n is set too high, the supporting moment will exceed the required moment, resulting in a larger effort than necessary. On the other hand, if n is set too low, the effort will be close to the required effort, indicating insufficient support. Table 2 reveals that the extension effort was significantly reduced by the strategy in comparison to flexion effort. However, in some trials, the flexion effort was reduced by less than 10% or even increased, which could potentially cause harm to the user. Therefore, the selection of n should be personalized based on the user's needs. It is important to note that if n is set too small, the supporting moment will be minimal, and if n is set too high, the supporting moment will exceed the required moment, both of which may cause problems.

After thorough testing and validation, the MLASCS appears to be a promising strategy for knee-assistive devices. The technique has demonstrated its ability to accurately predict the amount of supporting moments required based on recorded gait data. Additionally, the MLASCS has a high processing speed of approximately 165 observers/s, allowing it to estimate the amount of supporting moment for a single gait cycle in around 1.1 seconds while walking at a speed of 1.5 m/s. The results indicate that the walking effort can be significantly reduced to 63.4% when the percentage of support (n) is set at 0.7. These findings suggest that the MLASCS has the potential to improve the efficiency and safety of knee-assistive devices, although further research is needed to investigate its effectiveness across different users and conditions.

Chapter 4: Knee Device Prototype

This chapter presents a discussion on the conceptual design of a knee device, including joint alignment, human attachment, and the controlling system. The knee device should be able to support while walking and freely move in the walking angle range. The device should be designed for easy wear and remove, with a user-friendly human attachment mechanism that includes a mechanical emergency stop. The device joint should be aligned to the knee joint. The strength of the device must be validated to assess the possibility of breakage. The controlling system may have a safety function that can impower the system in case of emergency. To validate muscle activity, electromyography (EMG) sensors were utilized to test muscle activity levels when wearing the device, wearing without support, and not wearing the device.

Chapter 4.1: Device Design

The device can be divided into three main sections: leg attaching section, body device section, and joint section. The attachment parts were constructed using flexible materials to accommodate various leg shapes of the users. In order to ensure user safety, the device structure was designed to be durable and equipped with mechanical safety measures in case of actuator or coding failure. The joint design presented in this study utilized a single revolute joint due to the limited knee flexion required for walking. It should be noted that the device was designed to provide support for the right leg specifically.

Leg attachment section

The design process for the device began with the attachment parts, which are positioned at four locations on the human leg - two on the upper leg and two on the lower leg. The attaching position requires flexible material for fitting the leg shape, and it should be tightened with the leg for preventing relative movement between the leg and the device. To optimize the extension moment required for walking, the attachment parts were primarily aligned posteriorly, as indicated by the design shown in Figure 16. The attachment parts consisted of three components, as depicted in the figure. The first component, called the fitting, was attached to the human leg and secured in place with a strap. This component was fabricated using TPU filament and 3D printing technology, allowing it to partially flex to fit the wearer's leg shape. The second component, the fitting connector, was locked into the fitting with a transition fit and connected to the core of the device. This component required a hard and inflexible material and was therefore fabricated using PLA filament and 3D printing technology.

Although the fitting and fitting connector were connected with a transition fit, a fitting knot was still necessary to prevent movement in the assembly direction. This component, called the fitting knot, was used to obstruct any unwanted movement.

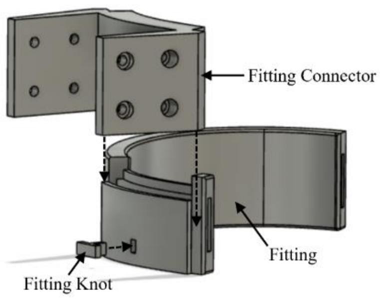

(a)

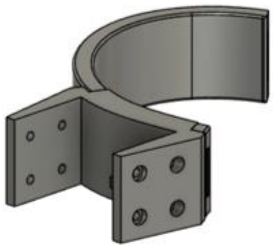

(b)

Figure 16 The component (a), and the assembled model of the attachment part (b).

Body device section

The body sections of the device serve as the frame components that connect all other sections together, similar to the chassis of a car. These parts consist of the top connector and the bottom connector for the upper and lower sections, respectively. Given their importance in supporting knee moment, these parts must be highly durable and not fragile, and were therefore constructed using PLA filament and 3D printing technology. As shown in Figure 17, the top and bottom connectors were attached to the fitting connector part using bolts and nuts. Once the fitting connector and the top/bottom connectors were securely connected, the fitting knot was used to lock all movement in place with a mechanical lock.

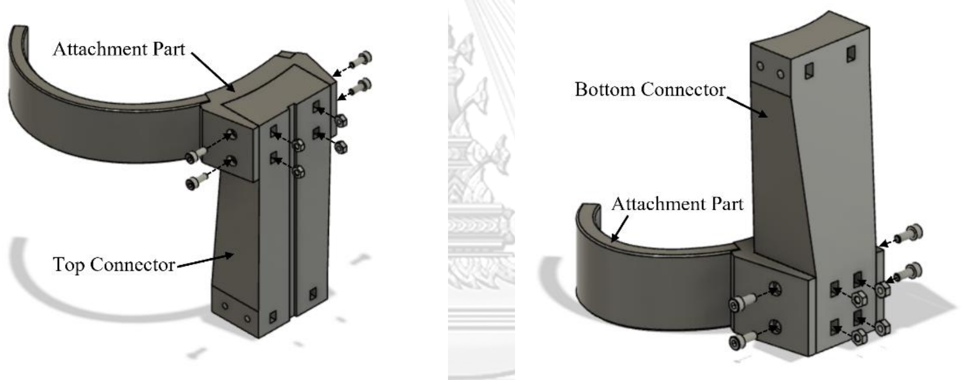

(a) (b)

Figure 17 The body and attachment section of upper part (a) and lower part (b).

Joint section

The joint component of the device was divided into two parts: the top motor connector and the bottom motor connector, as illustrated in Figure 18. The joint was designed as a single revolute joint that allows for free rotation during walking. However, to prevent harm in the event of actuator malfunction, it was deemed necessary to include a mechanical stop. The emergency stop mechanism was incorporated to halt device movement when the angle of the device is less than zero degrees.

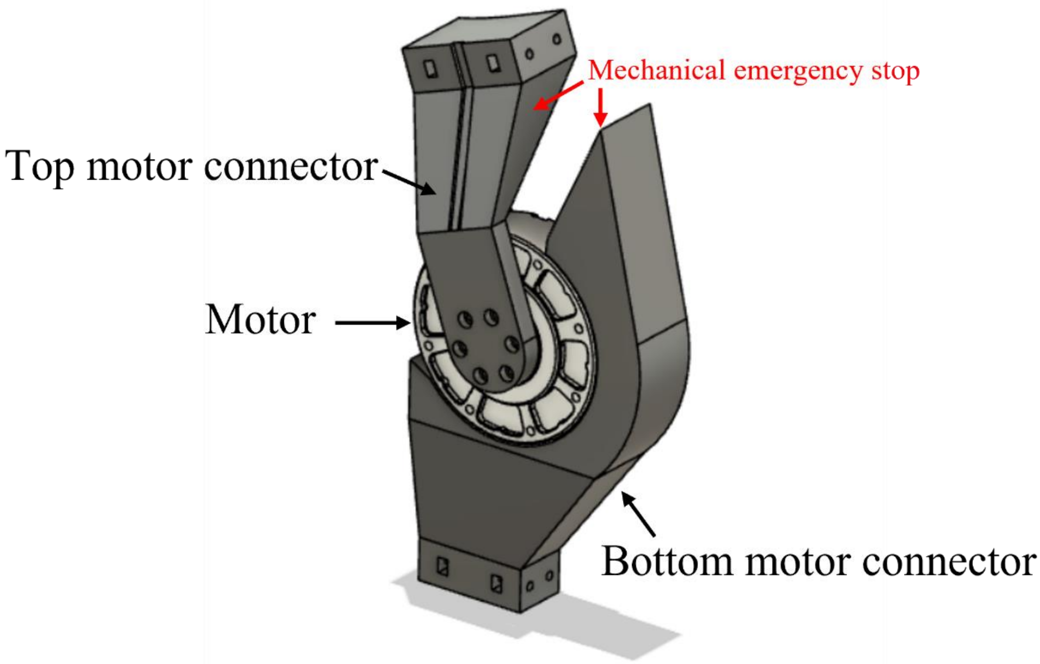

Figure 18 The joint part

The assembled device consists of an upper part and a lower part, each of which is composed of two attachment parts, a top/bottom connector, and a top/bottom motor connector, as shown in Figure 19. Figure 20 shows the built device when it is worn by the user.

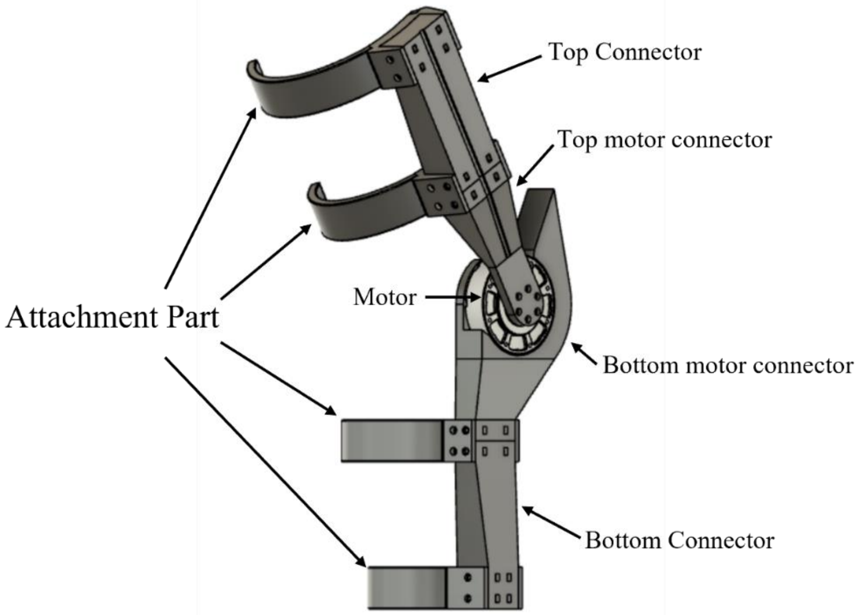

Figure 19 The assembled device.

(a) (b)

Figure 20 A sample wearing the built device and walk at the heel strike state (a), and the toe off state (b).

Chapter 4.2: Device strength

Because all sections were built by a 3D printing technology, strength validation is required. As the quality of printing may vary depending on the 3D printer, it is essential to conduct a study on the device's durability. Therefore, the device was separated into upper and lower parts for the durability study. While the infill density and pattern can be set during the building process, they do not necessarily guarantee the printing quality. Additionally, 3D CAD programs may have limited capabilities in analyzing 3D printed materials. For this study, the device was assumed to be built with 100% infill and analyzed only for safety factors. Table 2 shows the material properties of the PLA and TPU used in the study. Each part was loaded with 40 Nm, which is the maximum average knee moment during a gait cycle from previous calculation, at the position connecting to the motor. The attachment components were fixed, and bolts and nuts were added to connect all components, as shown in Figure 21. The results showed that the safety factor of both the upper and lower parts exceeded 15, indicating that the device is not likely to break during operation due to the input moment.

Table 3 Material properties of PLA and TPU

<table>
<tr><td rowspan="9">PLA</td><td colspan="2">Mechanical Properties</td></tr>
<tr><td>Young’s modulus</td><td>2.7 GPa</td></tr>
<tr><td>Poisson’s ratio</td><td>0.33</td></tr>
<tr><td>Shear modulus</td><td>1.5 GPa</td></tr>
<tr><td>Density</td><td>1.240 g/cm^3</td></tr>
<tr><td colspan="2">Strength</td></tr>
<tr><td>Yield strength</td><td>55 MPa</td></tr>
<tr><td>Tensile strength</td><td>45 MPa</td></tr>
<tr></tr>
<tr><td rowspan="8">TPU</td><td colspan="2">Mechanical Properties</td></tr>
<tr><td>Young’s modulus</td><td>0.8 GPa</td></tr>
<tr><td>Poisson’s ratio</td><td>0.45</td></tr>
<tr><td>Shear modulus</td><td>1.5 GPa</td></tr>
<tr><td>Density</td><td>1.120 g/cm^3</td></tr>
<tr><td colspan="2">Strength</td></tr>
<tr><td>Yield strength</td><td>30 MPa</td></tr>
<tr><td>Tensile strength</td><td>45 MPa</td></tr>
</table>

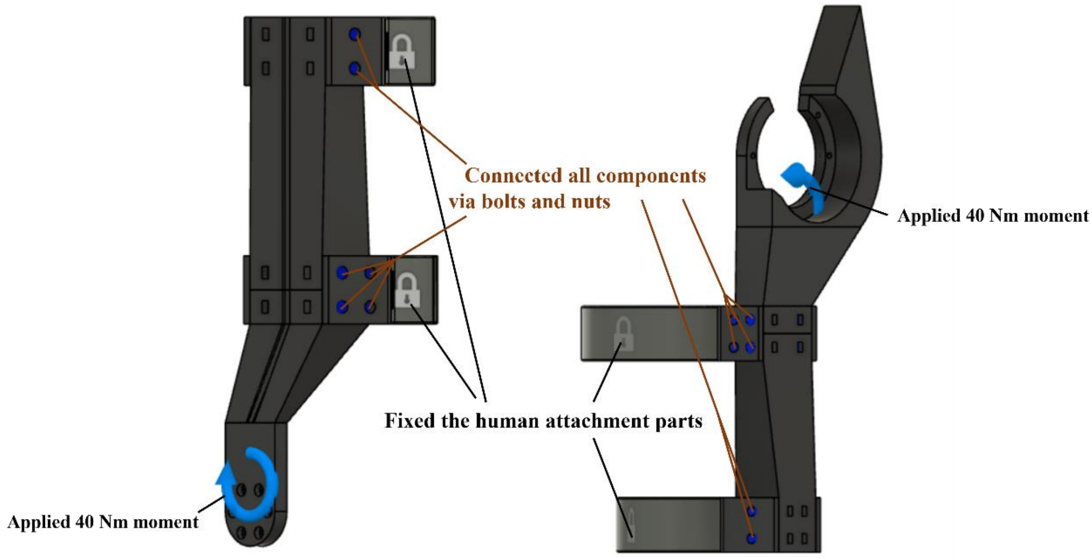

Figure 21 Load and constrain setting for durability test of the upper part (Left) and lower part (Right).

Chapter 4.3: Controlling System

The control system was divided into two main parts, namely the actuator and the control parts. The actuator part describes the motor utilized in the system, while the control part discusses the design of the control system used to command the actuator input, utilizing output feedback data from the actuator.

Actuator

The device utilized an actuator that was replicated from an MIT mini-cheetah servo motor (GIM8008 series), which can be directed to execute various commands such as position, velocity, torque, joint stiffness, and joint damping coefficient. The communication interface adopted by the device is the CAN-BUS communication protocol. The motor specification is shown in Appendix C. The motor is capable of generating a maximum moment of approximately 15 Nm. Although the highest recorded average knee moment during gait is 40 Nm, the device was designed to provide partial support to the knee moment due to safety concerns. Hence, the maximum moment of the motor which is around 40% of the maximum knee moment meets this requirement.

Control

In the MATLAB simulation section, a control concept was developed and verified. However, to implement this concept in real systems, further steps are necessary. While the k-nearest neighbor (kNN) model, classified by the Statistics and Machine Learning Toolbox in MATLAB version R2022b (MathWorks, Natick, MA, USA), was used in the simulation, the performance revealed that leading to system delays and latency, only 3-4 predictions possible in a single gait cycle which means the method is not fast enough to support gait. Additionally, discrepancies were observed between the knee angles and angular velocity feedback from the actuator and the data recorded by the motion capture system. For example, the maximum knee angle in the initial place is around 20 degrees, but 25 degrees when reading feedback from the motor. To address this, knee angles and angular velocities were re-recorded, and a new state classifier model was constructed. Finally, the accuracy of the new state classifier model needs to be verified before deployment.

Re-recording knee angle and angular velocity

The knee angle and omega data were recorded to observe the behavior of the motor in a gait cycle. A sample walked with the device at 1.5 m/s, matching the motion capture camera's speed. The recorded data is shown in Figure 22.

The knee omega in the initial place state is often observed within the range of 0 to around 150 deg/s while some data exceed 150 deg/s, but less than 250 deg/s. In the final place state, the observed knee omega range is smaller than the initial place state within -100 to 0 deg/s.

The knee angle range in the initial and final lift state is between 0 to 70 degrees, while the plot of the knee angle to the knee omega can be observed as a right-beveled circle. The maximum knee omega in the initial lift state is around 450 deg/s, and the minimum knee omega in the final lift state is around -400 deg/s.

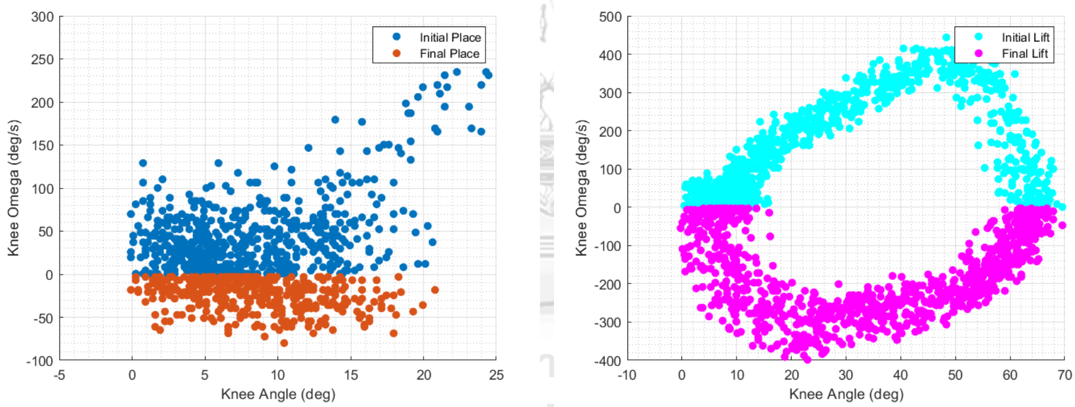

(a) (b)

Figure 22 The recorded knee angle and knee omega in the initial and final place state (a), and initial and final lift state (b).

State Classifier

The k-nearest neighbor (kNN) model was replaced with a faster if-else concept as it was found to be more efficient during MATLAB experiments. The state classifier was implemented using multiple if-else functions to predict the current state using the current knee angle and omega along with the latest predicted state. The predicted state and the current knee angle were then used to determine the appropriate stiffness for supporting the knee moment during walking, following the same equations as used in the simulation. To prevent hazardous moments for the wearer, the state classifier for controlling the device was designed to prevent movement if the feedback angle exceeded 70 degrees, the maximum observed knee angle from the Re-recording knee angle and angular velocity section.

The system's decision-making process involves checking the current knee angle (θ) at the beginning to determine the predicted state. At first, the starting state is the final lift state. Then, the state will operate with the following conditions. If θ is greater than 70 degrees, the predicted state is the same as the last predicted state. However, if θ is less than or equal to 70 degrees, the system checks if θ is greater than 25 degrees. If θ is greater than 25 degrees and the current knee omega (ω) is positive, then the initial lift state is predicted. On the other hand, if ω is negative, the predicted state is the final lift state.

If the knee angle θ is less than or equal to 25 degrees, the system follows a decision-making process in the order shown below, skipping the remaining steps if the state is already predicted. First, if the last predicted state is the final lift state and ω is greater than zero, the predicted state is the initial place state. However, if ω is less than zero, the predicted state remains the final lift state. Next, if the last predicted state is the initial place state and ω is greater than zero, the predicted state remains the initial place state. If ω is less than zero, the predicted state is the final place state. Lastly, if ω is greater than zero, the predicted state is the initial lift state, otherwise, the predicted state is the final place state.

The methods above are the if-else set that is used in the controlling system. Besides, Figure 23 summarizes the system as a state flow for easy understanding.

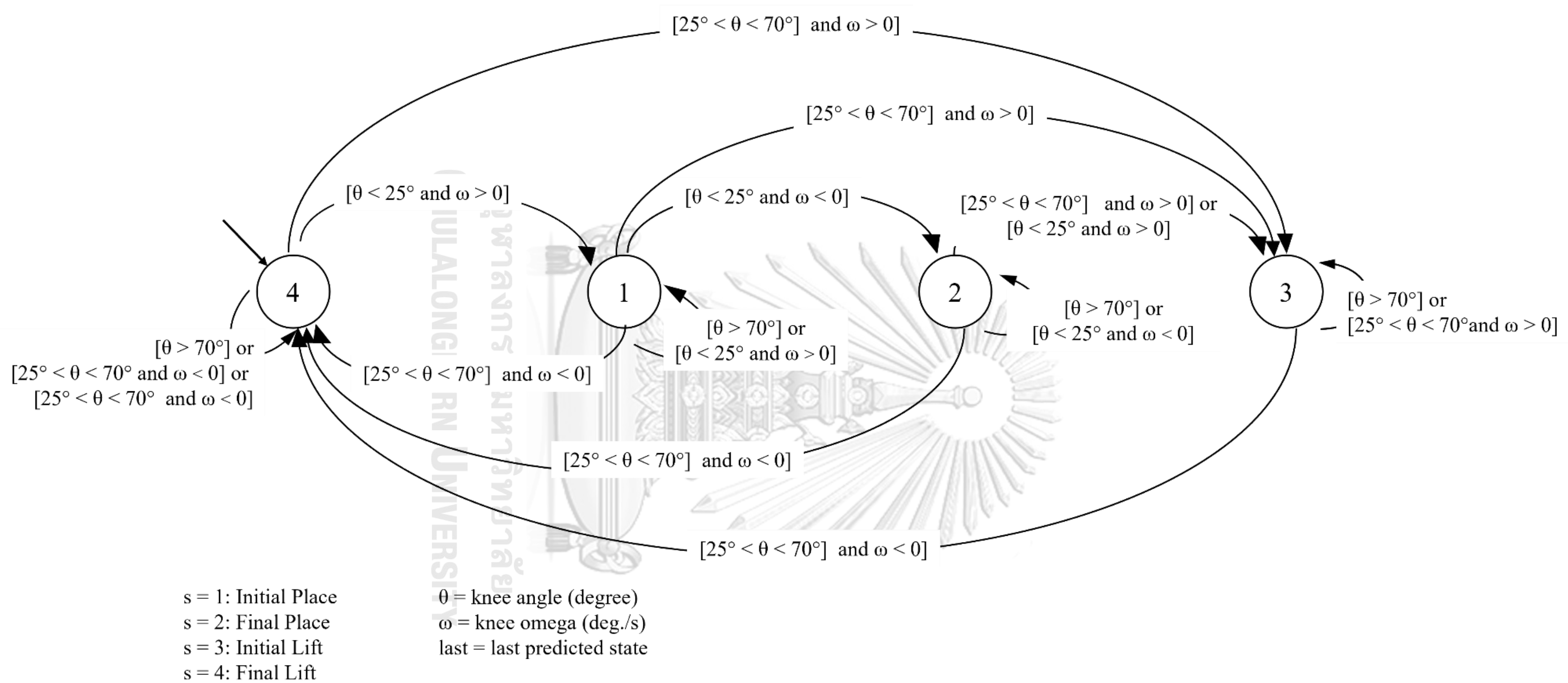

Figure 23 The structure of the state classifier

Validation of the state classifier

The state classifier created in Figure 23 needed to be validated before being used for real-time classification to support knee moments during walking. Validation was performed using the re-recorded data from the knee device passing through the state classifier to compare the correctness of the predicted state. The results showed that the accuracy of the classifier was around 98.6%, with the confusion chart displayed in Figure 24.

The validation of the state classifier was conducted using 2,974 data sets. The accuracy rate for the final place state was found to be 100%. However, in the final lift state, out of 955 data sets, only 935 were accurately predicted. It was also observed that in the initial lift state, out of 1,024 sets, only 4 were inaccurately predicted, and in the final place state, out of 592 sets, 18 were wrongly predicted.

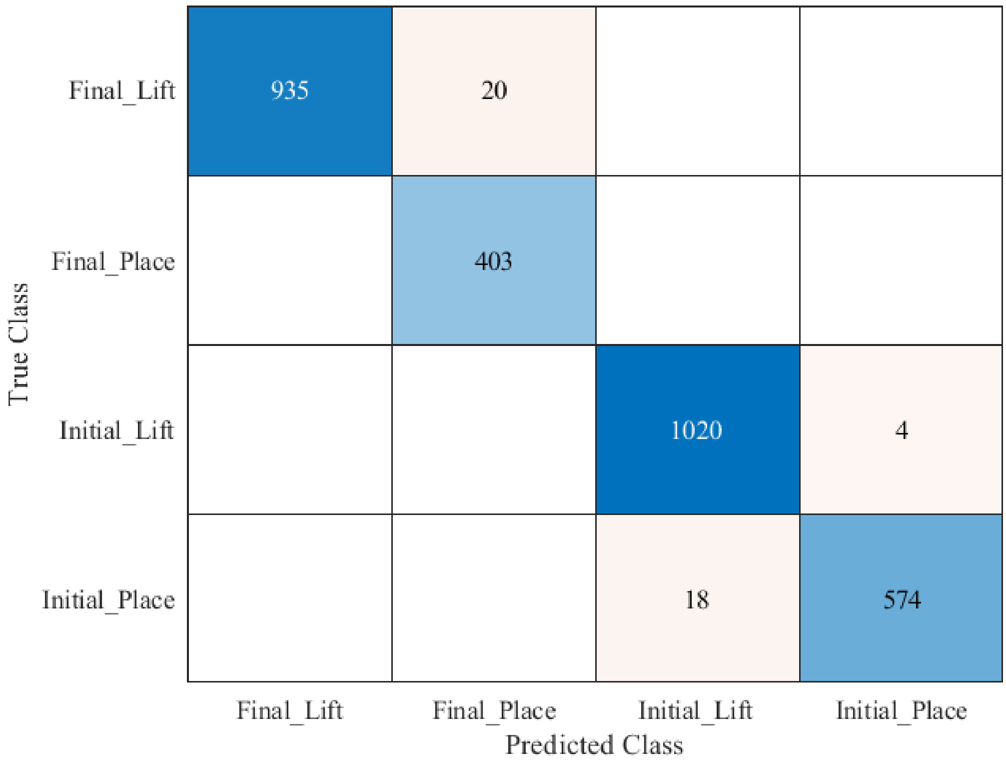

Figure 24 The confusion chart of the state classifier

Chapter 4.4: Performance evaluation of a knee device

To evaluate the performance of the control system and knee device, the real device needed to be validated when applying different percent of support. For this purpose, the electromyography (EMG) sensors were attached to the wearer's leg at the Rectus Femoris, Biceps Femoris, and Lateral Gastrocnemius muscle, as illustrated in Figure 25.

The experiment was designed to record in various conditions as walking without the device, walking with 0% assistance from the device, two trials of 10%, 20%, and 30% assistance from the device, and the maximal voluntary contraction (MVC) of each muscle for verifying the amount of the EMG signal when enforcing maximize exertion. The sample is a Thai male, 171 cm in height and 59.0 kg in weight, walking at a speed of 1.5 m/s. The maximum level of assistance in the experiment was 30% due to the limitation of the motor and safety. The EMG sensor used in the experiment is the COMETA wave plus wireless EMG system with mini wave waterproof unit with a sampling frequency 0f 2000Hz.

The muscle's maximum voluntary contraction (MVC) data was recorded, filtered using the banpass function in MATLAB to limit the raw data within the recommended frequency range of 10-1000 Hz [85], and sampled for 3 seconds. The plot of the MVC data can be seen in Figure 26.

Figure 25 The positions where the EMG sensors were attached.

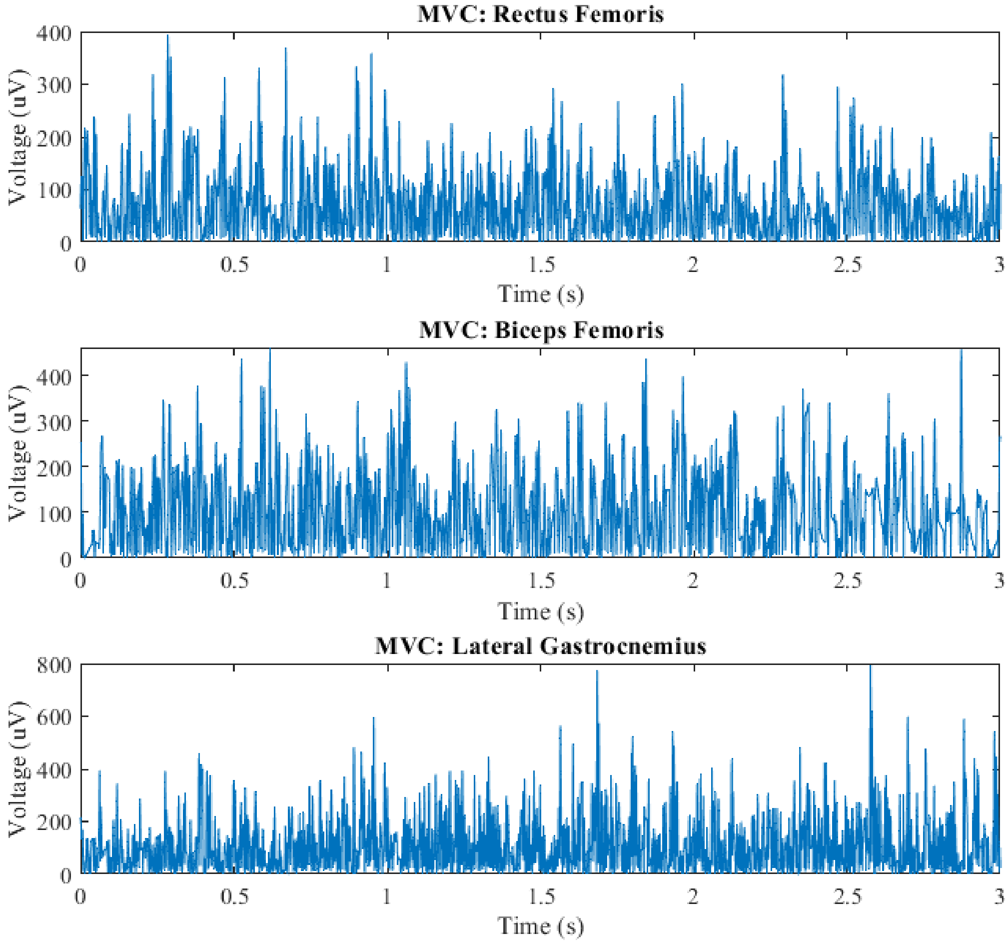

Figure 26 Plot of the maximal voluntary contraction (MVC) data of Rectus Femoris, Biceps Femoris, and Lateral Gastrocnemius muscle from the EMG sensors

The results of the EMG recordings from the experiments were processed by filtering within the frequency range of 10-1000 Hz and smoothing using the moving mean sample points, taking the absolute value, and sampling for 10 seconds. The plots of all the EMG walking data can be seen in Figure 27. The duration in each gait cycle is sometimes not the same, but as observed, it is around 1.1 seconds, which can be seen in each subfigure. For mapping to a gait cycle, the biceps femoris muscle shows a short period of activation right before the heel strike and once again during heel-off. Likewise, the lateral gastrocnemius muscle demonstrates a brief period of low-amplitude muscle activity immediately after the heel strike, followed by increased EMG activity towards the end of the stance phase [85].

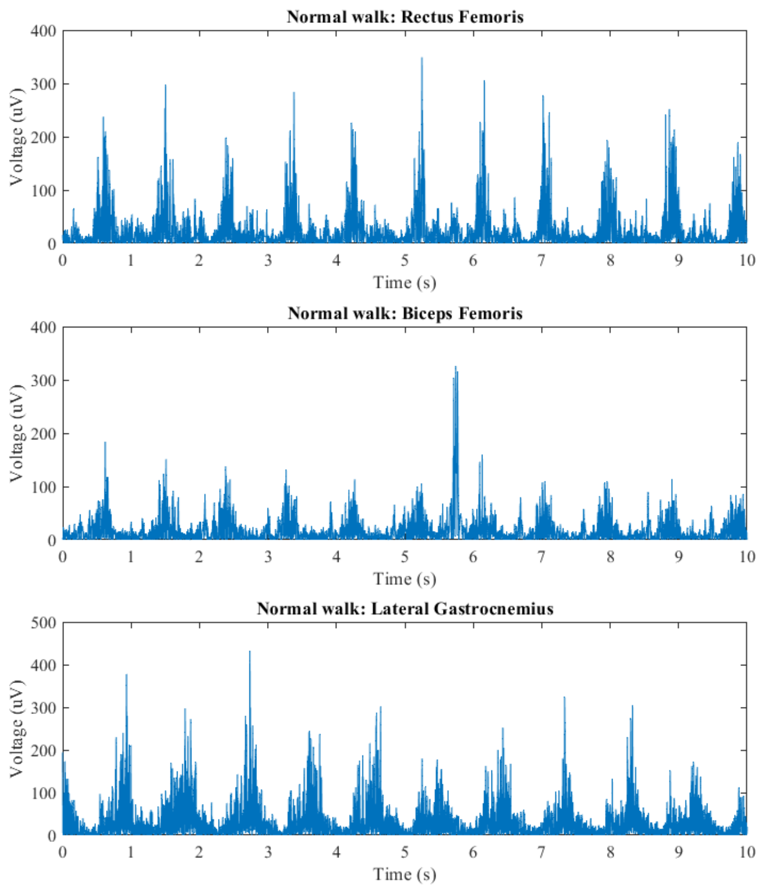
Normal walk: Rectus Femoris
Normal walk: Biceps Femoris
Normal walk: Lateral Gastrocnemius
Voltage (uV)
Time (s)

(a)

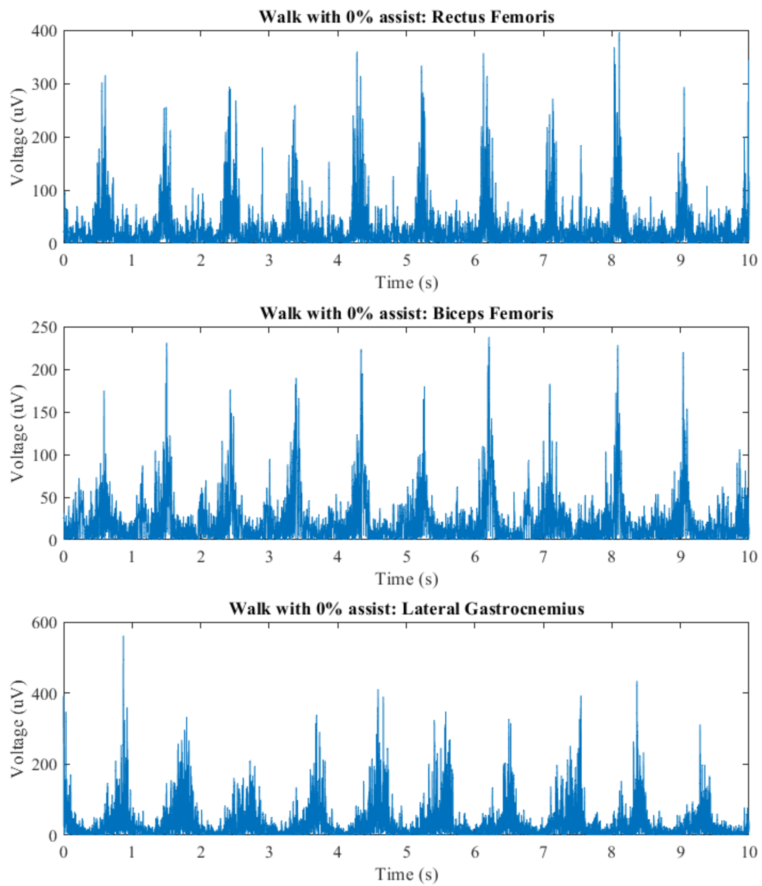
Walk with 0% assist: Rectus Femoris
Walk with 0% assist: Biceps Femoris
Walk with 0% assist: Lateral Gastrocnemius
Voltage (uV)
Time (s)

(b)

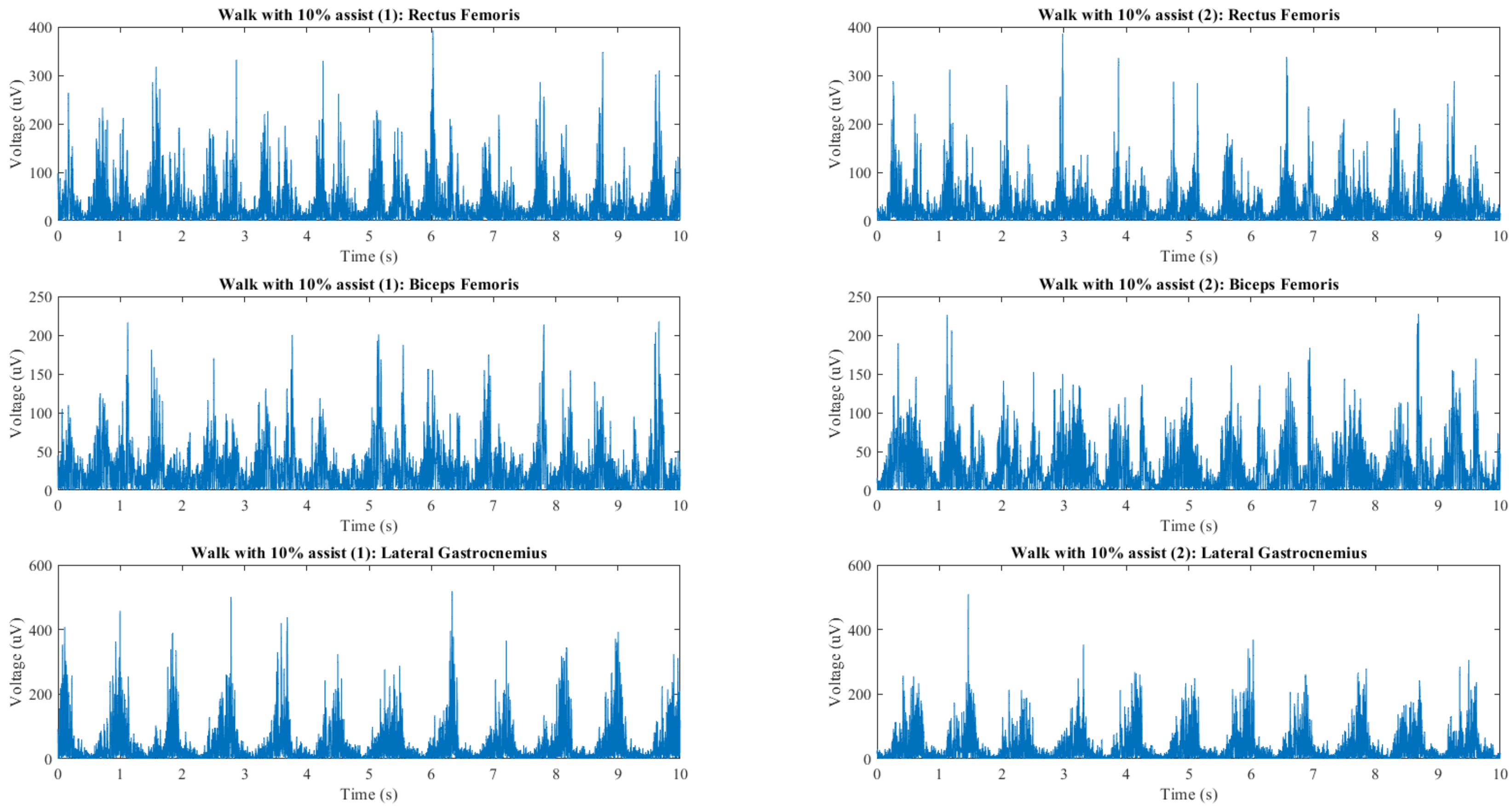
Walk with 10% assist (1): Rectus Femoris
Walk with 10% assist (2): Rectus Femoris
Walk with 10% assist (1): Biceps Femoris
Walk with 10% assist (2): Biceps Femoris
Walk with 10% assist (1): Lateral Gastrocnemius
Walk with 10% assist (2): Lateral Gastrocnemius
Voltage (uV)
Time (s)

(c)

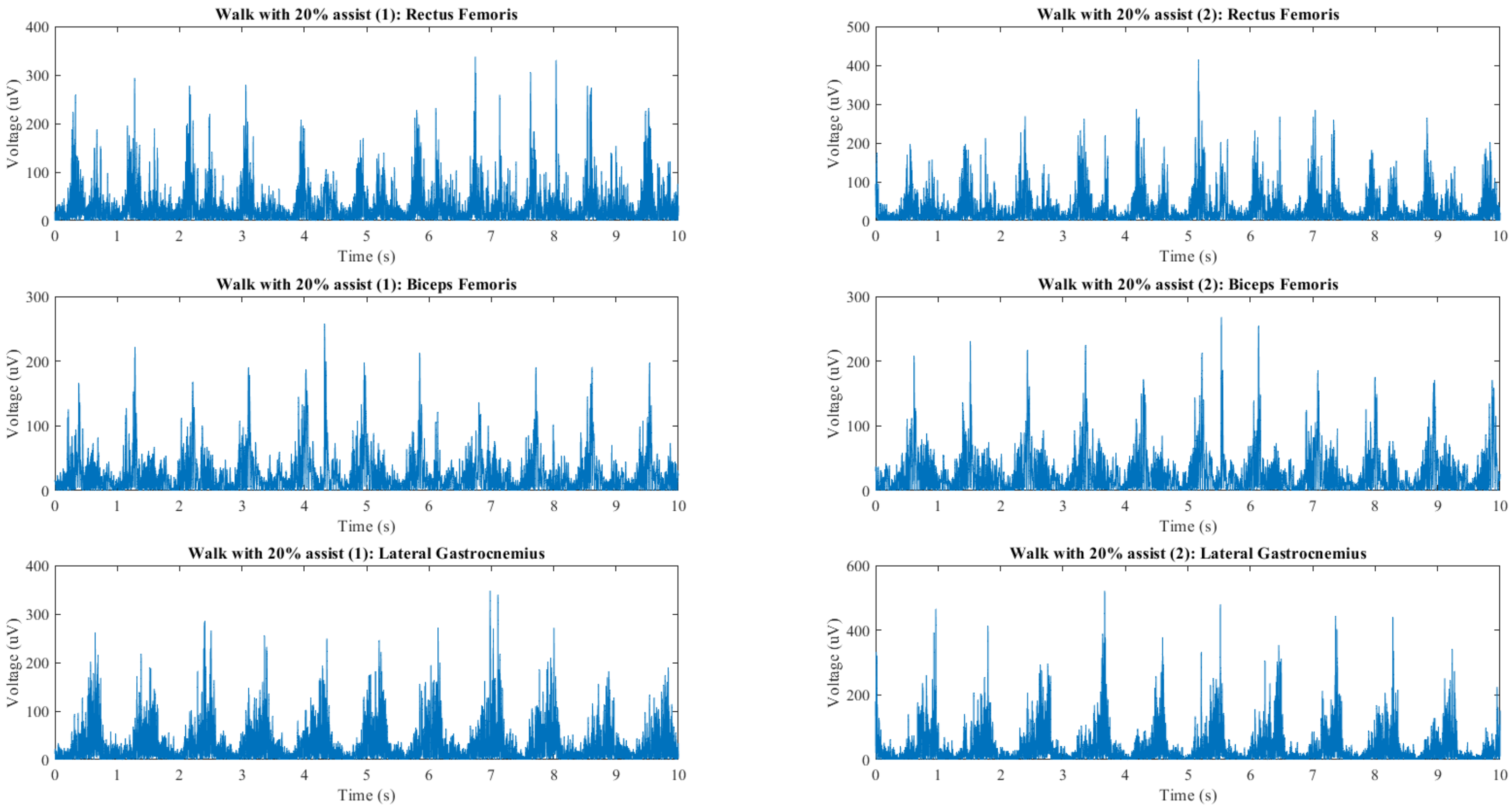
Walk with 20% assist (1): Rectus Femoris
Walk with 20% assist (1): Biceps Femoris
Walk with 20% assist (1): Lateral Gastrocnemius
Walk with 20% assist (2): Rectus Femoris
Walk with 20% assist (2): Biceps Femoris
Walk with 20% assist (2): Lateral Gastrocnemius
Voltage (uV)
Time (s)

(d)

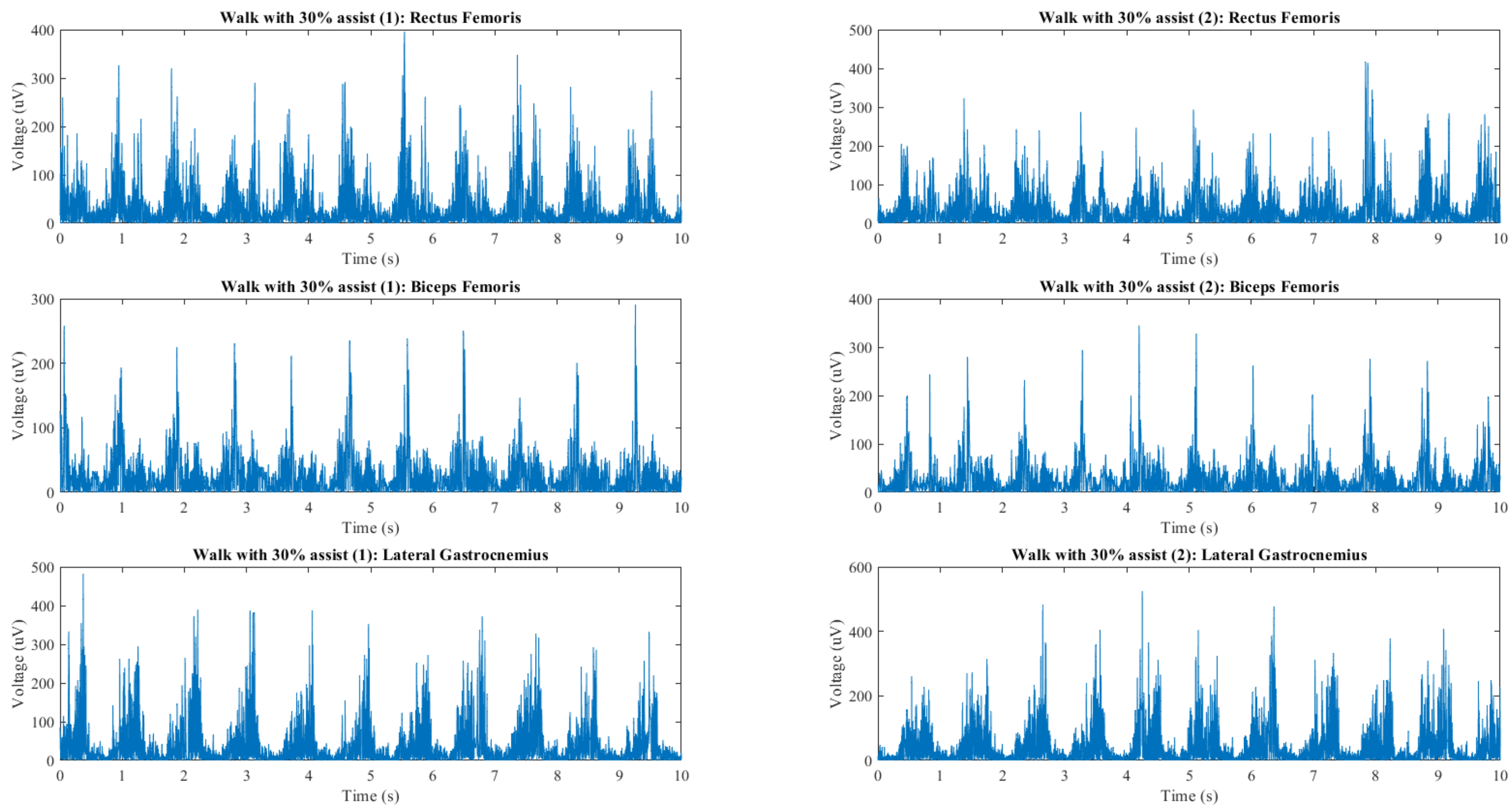

(e)

Figure 27 The plot of EMG walking data in normal walking without device (a), walking with 0% assist from device(b), and 2 trials of walking with 10% assist from device (c), walking with 20% assist from device (d), walking with 30% assist from device (e)

The amplitude of all three muscles during the walk with 0% assist condition tends to be higher than the normal walk, as observed in figure 27(a) and (b). This is because the device has weight and sometimes moves relatively to the leg due to deformable muscle at the attachment parts. The weight and friction of the device cause load to the muscle, and the muscle power is enlarged for walking with these burdens.

In the case of the walk with 10% assist condition, the peak amplitude of the rectus femoris is quite similar in both trials. However, some differences can be observed between each trial at the biceps femoris and lateral gastrocnemius. In trial 2, the peak amplitude tends to be lower than in trial 1. Additionally, the amplitude of the base band at the biceps femoris in trial 2 seems to be higher, while the amplitude of the base band at the lateral gastrocnemius is quite similar in both trials.

For the walk with 20% assist condition, the peak amplitudes at the lateral gastrocnemius in trial 2 are clearly observed to be higher than in trial 1. The peak amplitude at the rectus femoris and biceps femoris in trial 2 is also higher than in trial 1. However, the base shape is quite the same at all three muscles.

Similarly, in the case of the walk with 30% assist condition, the peak amplitudes at the lateral gastrocnemius in trial 2 are clearly observed to be higher than in trial 1. The signal shape at the rectus femoris and biceps femoris is quite similar, but some high peak amplitudes can be observed in trial 2.

It should be noted that these observations provide a skim description of the signal characteristics, and all the signals require additional processing before comparison with each other. One effective method for easy comparison is to use the root mean square (RMS) equation for all signals and compare their performance using the RMS value.

Chapter 4.5: Performance Results and Discussion

The knee device prototype was validated using EMG sensors to measure its performance. The MVC data of the participant's Rectus Femoris, Biceps Femoris, and Lateral Gastrocnemius muscles were recorded, and their root mean square (rms) values were 99.0, 136.8, and 158.4, respectively. Table 4 shows a comparison of the rms values in different conditions. "Normal walking" is the rms value during walking without wearing the device. "Power 0%" is the rms value when wearing the device with 0% support. The rms values for 10%, 20%, and 30% supported by the device are displayed as "Power 10%", "Power 20%", and "Power 30%", respectively, and each condition was tested twice. All data are also compared as a percentage of MVC as seen in “%MVC” row.

Table 4 Comparison of the rms in each condition

	Rectus Femoris (μV)	Bicep Femoris (μV)	Lateral Gastrocnemius (μV)
MVC	99.0	136.8	158.4
%MVC	**100%**	**100%**	**100%**
Normal walking	44.3	30.0	53.1
%MVC	**44.7%**	**21.9%**	**33.5%**
Power 0%	53.5	36.1	62.8
%MVC	**54.0%**	**26.4%**	**39.6%**
Power 10%			
Trial 1	57.1	40.0	72.4
Trial 2	50.0	43.0	58.4
Average	53.6	41.5	65.4
%MVC	**54.1%**	**30.3%**	**41.3%**
Power 20%			
Trial 1	50.5	40.7	50.3
Trial 2	52.9	42.2	65.8
Average	51.7	41.4	58.0
%MVC	**52.2%**	**30.3%**	**36.6%**
Power 30%			
Trial 1	57.9	42.3	66.6
Trial 2	60.7	45.4	73.5
Average	59.3	43.8	70.0
%MVC	**59.9%**	**32.0%**	**44.2%**

The table indicates that the %MVC increases in all positions after wearing the device due to its weight and friction between the wearer's leg and the device. The %MVC of the Rectus Femoris is almost the same at 10% support, decreases at 20%, but increases at 30% support. The %MVC of the Biceps Femoris is consistently higher than the Power 0% condition, indicating no assistance from the device. The device assists the Lateral Gastrocnemius muscle only at 20% support but assimilates at 10% and 30%. However, factors such as imperfect gait cycles, communication delays, and misalignment may affect the device's performance. Therefore, the wearer needs to get accustomed to the device and understand its effects on supporting knee moments during walking.

Chapter 5: Conclusions

The aim of this study was to develop a knee assistive device that would provide support during walking. The device was constructed in two parts: a control algorithm and a device prototype. The success of the device was contingent upon an effective control system and a prototype that would be comfortable for the user. Data on the position of the hip, knee, ankle, finger, and ground reaction force (GRF) were collected from three adult Thai participants with an average age of 23, a height of 171-172 cm, and a weight of 51.9-61.8 kg, walking at a speed of 1.5 m/s. The data were used to calculate ankle and knee angle, angular velocity, and angular acceleration, which were then used to determine knee moment required for walking.

The Machine Learning and Artificial Stiffness Control Strategy (MLASCS) was used to command the proper amount of support moment needed to assist with walking. The MLASCS comprised a trained machine learning model and the instantaneous artificial stiffness per body mass (IASPB) equations. The trained model classified the state of a gait cycle by using knee angle and omega, with an accuracy of approximately 99.9%. The IASPB equations mapped the amount of stiffness required to support the knee moment based on the knee angle and state. The user could adjust the percentage of support (n) to select the amount of assistance needed. Validation of the MLASCS with nine trial datasets showed that it could reduce the total effort over a gait cycle by up to 63.4% when the n was 0.7 by simulation.

Using the MLASCS as a basis, a posterior-support device was designed using 3D printing filament. The device was tested for durability and was found to have a safety factor greater than 15 when applying 40 Nm, indicating that it would not break during operation. The control system used an actuator that was replicated from an MIT mini-cheetah servo motor, which could command position, velocity, torque, joint stiffness, and joint damping coefficient, and provide feedback on current position, velocity, and torque. While the MLASCS could predict up to 165 observers per second, the latency time increased significantly when connecting the microcontroller to the device. As a result, the if-else method was selected as the classifier instead of the MLASCS. The walking data in knee angle and angular velocity had to be re-recorded to obtain the actual angle and velocity from the motor, which were required to build a classifier. The state classifier was created using knee angle, knee angular velocity, and the latest predicted state as inputs to classify the state. The predicted state and knee angle were then used to determine the amount of stiffness required to support the knee moment, as in the simulation section.

The performance of the knee device was conducted using electromyography (EMG) sensors attached to the Rectus Femoris, Biceps Femoris, and Lateral Gastrocnemius muscles. The test was conducted under various conditions, including the maximal voluntary contraction (MVC) of each muscle, normal walking without the device, walking with 0% assistance from the device, and two trials of 10%, 20%, and 30% assistance from the device. The root mean square (rms) results showed that the data when the device assisted the knee moment was mixed between increased and decreased muscle activity, indicating that the device was sometimes helpful and sometimes not helpful. This may be due to an imperfect gait cycle, motor command delays, and misalignment of the device. Further data collection and validation with more samples, including an increasing amount of support, are necessary to verify the usefulness of the device.

Appendix A: Plot of CG velocity

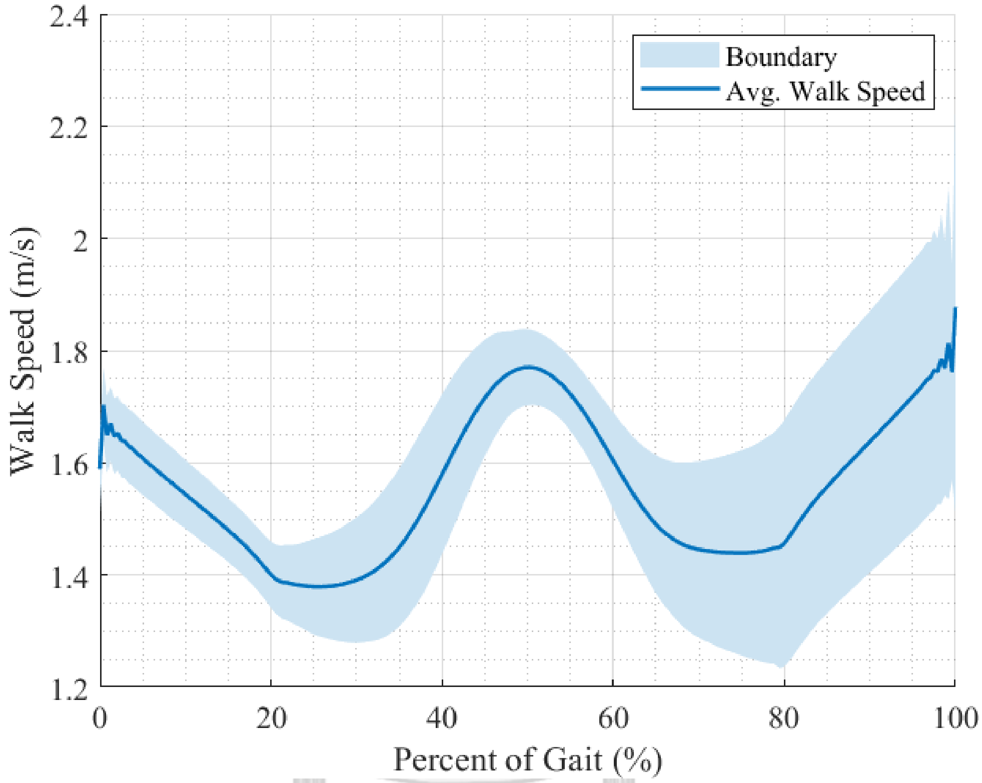

Figure A1 Plot of CG velocity which represents walking speed.

Appendix B: Data used for calculation.

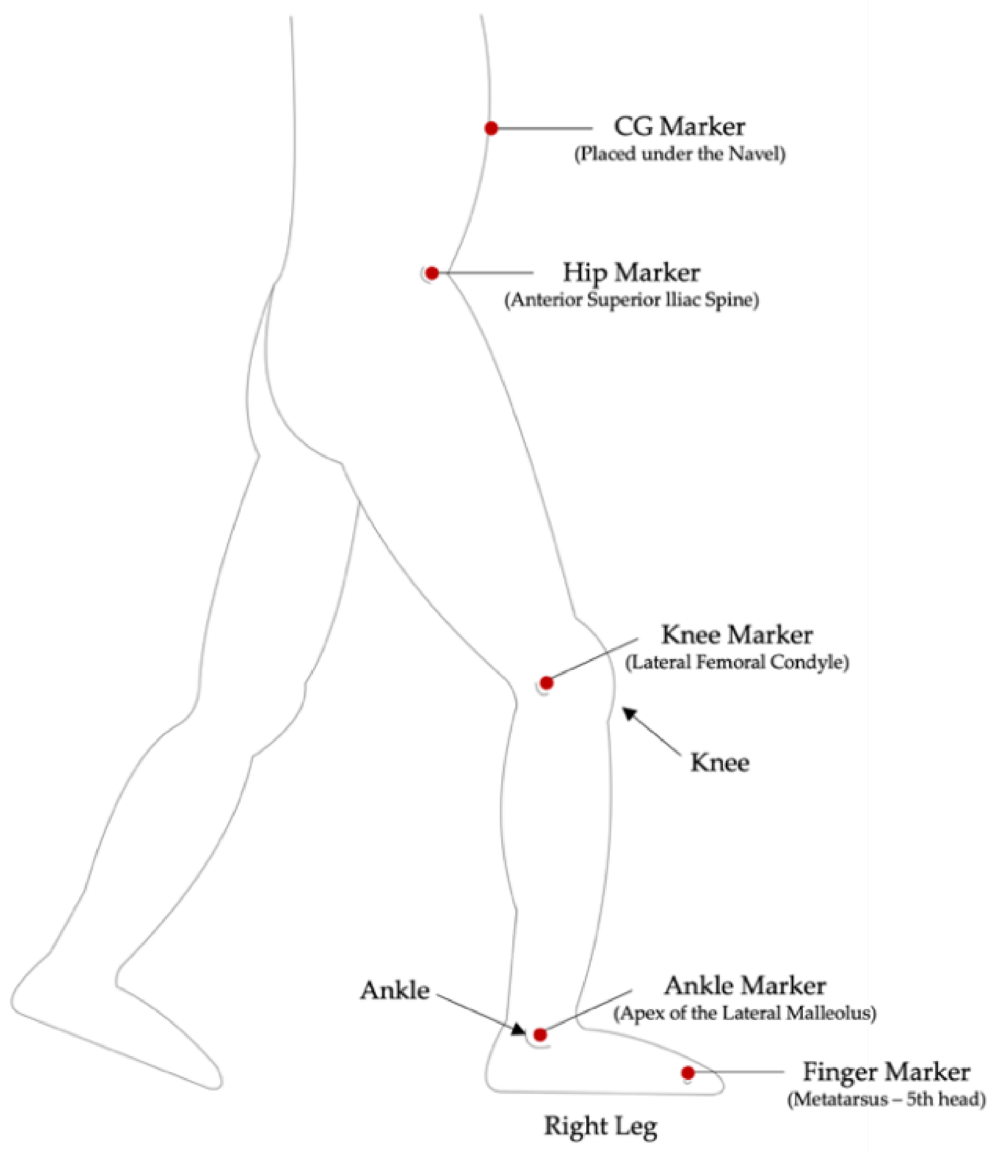

Figure B.1 Position of Marker

*The data shown in all tables start from Heel Strike position.

Table B.1. The average knee and ankle angle, angular velocity, and angular acceleration data

Frame	Ankle			Knee		
	Angle (deg)	Omega (deg/s)	Alpha (deg/s^2)	Angle (deg)	Omega (deg/s)	Alpha (deg/s^2)
1	98.96366	138.5484	-2244.34	5.890337	146.3732	-877.26
2	107.1243	138.6703	-2405.49	7.004967	152.9565	-951.717
3	104.7526	123.2988	-2315.01	7.527775	144.2685	-937.856
4	106.9952	114.9021	-2325.27	8.289025	142.29	-962.505
5	106.4379	102.6327	-2267.46	8.876192	136.2901	-962.834
6	107.5767	93.06269	-2250.5	9.540421	132.7714	-976.403
7	107.5584	82.0365	-2199.34	10.12225	127.613	-978.886
8	108.1823	72.17959	-2184.27	10.72067	123.4337	-985.155
9	108.3489	61.86754	-2137.12	11.27541	118.6433	-985.717
10	108.6878	51.94152	-2167	11.82077	114.175	-985.718
11	108.8748	41.842	-2149.62	12.33948	109.561	-982.231
12	109.0191	31.35934	-2350.83	12.83659	104.978	-976.046
13	109.1271	20.06472	-2521.6	13.31383	100.4463	-967.044
14	109.1916	6.247	-3397.65	13.77112	95.97666	-955.032
15	109.1989	-9.57408	-3148	14.20945	91.58504	-939.197
16	109.1229	-21.6414	-2054.81	14.62492	87.26129	-924.154
17	109.0025	-31.1038	-2048.1	15.02091	83.05176	-893.812
18	108.8282	-40.4645	-1903.42	15.39704	78.92581	-882.104
19	108.6211	-48.1495	-1282.17	15.7553	74.97069	-828.803
20	108.3843	-52.3478	-585.412	16.09563	71.08329	-842.477

Frame	Ankle			Knee		
	Angle (deg)	Omega (deg/s)	Alpha (deg/s^2)	Angle (deg)	Omega (deg/s)	Alpha (deg/s^2)
21	108.1467	-55.1841	-657.457	16.41985	67.37491	-775.265
22	107.88	-57.9181	-518.569	16.72476	63.40197	-949.563
23	107.6061	-60.3118	-520.421	17.01011	58.93997	-1063.08
24	107.3052	-62.475	-419.748	17.26851	51.15346	-2308.77
25	106.9987	-64.2598	-367.353	17.47931	40.0746	-2210.32
26	106.6946	-65.7513	-290.284	17.64496	32.01664	-1341.65
27	106.3939	-66.9103	-222.997	17.78115	25.46221	-1505.69
28	106.0733	-67.7266	-145.36	17.88337	18.93604	-1294.64
29	105.7581	-68.2122	-78.7734	17.9586	12.98049	-1266.13
30	105.4413	-68.3928	-13.707	18.0072	7.426724	-1119.89
31	105.1354	-68.3005	44.2976	18.03297	2.358397	-1062.1
32	104.8153	-67.9457	99.53256	18.03287	-2.36646	-975.141
33	104.5053	-67.3767	140.68	18.01278	-6.78656	-934.308
34	104.1891	-66.6481	171.6969	17.97125	-11.0173	-893.567
35	103.8794	-65.7679	210.392	17.91102	-15.0949	-868.959
36	103.5547	-64.6806	256.6163	17.82916	-19.0672	-844.59
37	103.2495	-63.3831	304.826	17.73128	-22.9189	-817.355
38	102.963	-61.8761	349.4348	17.61769	-26.6322	-784.677
39	102.6981	-60.1872	386.6592	17.48944	-30.1854	-747.781
40	102.4265	-58.3362	417.1705	17.34313	-33.5541	-709.043
41	102.1661	-56.3608	440.2184	17.18207	-36.7428	-669.892
42	101.8949	-54.2855	453.8517	17.00349	-39.7503	-631.442

Frame	Ankle			Knee		
	Angle (deg)	Omega (deg/s)	Alpha (deg/s^2)	Angle (deg)	Omega (deg/s)	Alpha (deg/s^2)
43	101.6419	-52.1695	459.3558	16.81262	-42.5827	-593.567
44	101.3949	-50.0375	459.7197	16.60822	-45.239	-555.901
45	101.1683	-47.9153	455.9894	16.39337	-47.7277	-519.005
46	100.9523	-45.821	446.6586	16.16776	-50.0482	-481.316
47	100.7506	-43.7888	429.2376	15.93247	-52.1941	-441.278
48	100.5423	-41.8546	401.5226	15.68582	-54.1391	-396.319
49	100.3507	-40.0665	368.8716	15.43181	-55.8674	-346.114
50	100.1753	-38.4356	335.3251	15.17143	-57.3596	-292.505
51	100.0119	-36.9716	297.1915	14.90522	-58.5983	-235.29
52	99.82625	-35.6882	250.9119	14.62923	-59.5532	-173.534
53	99.65356	-34.6376	198.3677	14.35053	-60.2172	-107.323
54	99.4854	-33.8357	143.0307	14.06945	-60.5712	-37.487
55	99.33429	-33.3063	83.05333	13.78927	-60.599	35.91539
56	99.18212	-33.0714	15.69789	13.50959	-60.2743	112.5792
57	99.0366	-33.1633	-56.2425	13.23331	-59.5897	191.2664
58	98.88167	-33.5895	-129.988	12.95991	-58.5382	270.0916
59	98.72581	-34.3496	-199.188	12.69238	-57.1241	347.441
60	98.54974	-35.4093	-261.71	12.42977	-55.3478	422.3679
61	98.38058	-36.7507	-317.517	12.17772	-53.2342	493.7893
62	98.20492	-38.3307	-363.426	11.93593	-50.7973	560.2021
63	98.0339	-40.0975	-394.768	11.70764	-48.0688	620.2857
64	97.83716	-41.9696	-413.231	11.49101	-45.0746	672.8765

Frame	Ankle			Knee		
	Angle (deg)	Omega (deg/s)	Alpha (deg/s^2)	Angle (deg)	Omega (deg/s)	Alpha (deg/s^2)
65	97.63418	-43.8981	-418.037	11.28915	-41.8568	716.7996
66	97.41702	-45.8113	-408.075	11.10189	-38.454	751.8311
67	97.19705	-47.6652	-391.693	10.93131	-34.9073	778.0459
68	96.96872	-49.4468	-375.032	10.77747	-31.2511	795.1126
69	96.74311	-51.1466	-352.765	10.64193	-27.5371	803.4361
70	96.50755	-52.7242	-323.784	10.52336	-23.8055	803.9287
71	96.27142	-54.1652	-292.132	10.42275	-20.0882	797.2404
72	96.00076	-55.4298	-253.98	10.33605	-16.4142	784.1244
73	95.73183	-56.5034	-208.347	10.26723	-12.8133	766.0861
74	95.46615	-57.3475	-154.333	10.21597	-9.3058	743.8167
75	95.20452	-57.9412	-100.162	10.18173	-5.90776	718.3834
76	94.92598	-58.2734	-43.3778	10.16137	-2.6272	690.4423
77	94.65113	-58.3177	24.64712	10.15655	0.518577	659.9215
78	94.37466	-58.0282	98.42199	10.16545	3.517713	626.4575
79	94.11418	-57.3922	176.2365	10.18953	6.355127	590.399
80	93.85481	-56.379	260.3839	10.22625	9.015437	552.8175
81	93.6088	-54.9627	350.002	10.27591	11.50053	515.4478
82	93.35254	-53.123	440.5608	10.33427	13.81222	479.344
83	93.10505	-50.8613	531.0981	10.40298	15.9592	445.6435
84	92.85394	-48.1763	617.6862	10.47986	17.95962	415.7426
85	92.62859	-45.0992	702.3485	10.56716	19.83318	391.2785
86	92.43177	-41.6228	791.2006	10.66453	21.60867	373.1179

Frame	Ankle			Knee		
	Angle (deg)	Omega (deg/s)	Alpha (deg/s^2)	Angle (deg)	Omega (deg/s)	Alpha (deg/s^2)
87	92.26442	-37.7209	885.3804	10.77149	23.3181	361.9306
88	92.10228	-33.3812	980.0046	10.88435	24.98398	357.9499
89	91.96065	-28.608	1070.546	11.00474	26.64827	360.7892
90	91.83484	-23.4115	1158.153	11.13215	28.33916	369.4987
91	91.7392	-17.8123	1244.083	11.26817	30.08483	383.7432
92	91.65708	-11.808	1328.656	11.41112	31.90657	403.5003
93	91.6164	-5.43118	1402.543	11.56432	33.83678	428.595
94	91.60656	1.239405	1457.937	11.72653	35.89253	456.6915
95	91.63568	8.139846	1502.055	11.89949	38.08495	485.5892
96	91.68106	15.23477	1544.595	12.08049	40.39873	513.7801
97	91.76747	22.53295	1588.067	12.27356	42.84088	540.353
98	91.89625	30.02652	1625.677	12.4794	45.40711	566.409
99	92.06783	37.69286	1658.971	12.69862	48.09687	592.1142
100	92.25838	45.50914	1690.859	12.92853	50.89719	616.1889
101	92.4928	53.48876	1727.4	13.17272	53.80854	637.5281
102	92.74891	61.63966	1769.472	13.42807	56.8022	654.4059
103	93.05325	70.01085	1819.977	13.69903	59.87306	669.0834
104	93.39621	78.61717	1876.931	13.98377	63.00465	685.0885
105	93.78814	87.50122	1938.226	14.28439	66.22149	704.3701
106	94.21674	96.6799	2011.171	14.5992	69.53668	729.1398
107	94.69175	106.2411	2102.377	14.9302	72.99193	763.3321
108	95.19943	116.2785	2213.904	15.2762	76.63359	810.1339

Frame	Ankle			Knee		
	Angle (deg)	Omega (deg/s)	Alpha (deg/s^2)	Angle (deg)	Omega (deg/s)	Alpha (deg/s^2)
109	95.76561	126.8801	2341.213	15.64139	80.5349	871.2584
110	96.39656	138.1303	2485.744	16.02787	84.77005	946.9051
111	97.09193	150.1214	2651.907	16.43691	89.40638	1036.838
112	97.8143	162.8446	2832.422	16.86231	94.44983	1139.39
113	98.59569	176.3858	3004.905	17.31172	99.99136	1252.08
114	99.43599	190.6504	3140.087	17.7873	106.0742	1371.234
115	100.3518	205.4161	3209.597	18.2939	112.7273	1493.152
116	101.3347	220.3351	3198.04	18.83299	119.9493	1614.339
117	102.4013	235.0523	3109.409	19.40989	127.7501	1732.369
118	103.5351	249.2045	2959.699	20.02444	136.0885	1844.369
119	104.7419	262.6006	2776.98	20.68111	144.9497	1948.881
120	105.9931	275.0927	2585.336	21.37653	154.2559	2043.933
121	107.3093	286.7289	2397.314	22.11814	163.9945	2127.911
122	108.6659	297.487	2211.935	22.903	174.0736	2197.554
123	110.08	307.3938	2013.582	23.73754	184.4544	2249.224
124	111.5175	316.2668	1776.764	24.61642	194.9937	2278.485
125	113.0015	323.9191	1472.841	25.5465	205.6278	2282.087
126	114.5189	329.964	1076.639	26.52724	216.2286	2256.541
127	116.0753	333.9479	571.0208	27.56088	226.665	2198.766
128	117.6422	335.2996	-55.977	28.64052	236.7429	2106.957
129	119.2157	333.4435	-806.915	29.76821	246.3275	1979.842
130	120.7648	327.8115	-1664.92	30.93707	255.2213	1816.987

Frame	Ankle			Knee		
	Angle (deg)	Omega (deg/s)	Alpha (deg/s^2)	Angle (deg)	Omega (deg/s)	Alpha (deg/s^2)
131	122.2815	317.9655	-2601.24	32.14692	263.2847	1619.656
132	123.7105	303.5625	-3573.05	33.38498	270.3038	1389.158
133	125.0744	284.6329	-4530	34.6569	276.2013	1128.54
134	126.3581	261.3661	-5424.92	35.95883	280.8533	840.9934
135	127.533	234.137	-6223.14	37.28188	284.1281	530.6689
136	128.5516	203.4737	-6902.08	38.60821	285.8758	203.1578
137	129.4225	169.9516	-7447.52	39.93983	286.0739	-136.179
138	130.1248	134.1847	-7851.38	41.26809	284.666	-481.547
139	130.6658	96.89252	-8105.53	42.5894	281.6631	-826.482
140	131.0294	58.7413	-8208.89	43.89394	277.0547	-1164.8
141	131.23	20.48192	-8159.85	45.17937	270.9211	-1490.54
142	131.2325	-17.1575	-7959.02	46.42502	263.275	-1798.06
143	131.0716	-53.5016	-7617.59	47.63536	254.2605	-2083.24
144	130.7237	-87.9194	-7141.36	48.79283	243.9482	-2341.49
145	130.233	-119.781	-6537.84	49.9034	232.5213	-2569.85
146	129.6097	-148.539	-5828.75	50.96121	220.1178	-2767.28
147	128.8716	-173.795	-5042.97	51.9637	206.8784	-2933.07
148	128.0026	-195.257	-4210.2	52.89389	192.899	-3066.27
149	127.052	-212.786	-3359.34	53.76138	178.3787	-3168.23
150	126.0279	-226.401	-2525.43	54.5615	163.4319	-3240.62
151	124.965	-236.268	-1744.99	55.29775	148.2236	-3285.65
152	123.8471	-242.646	-1034.05	55.95344	132.8607	-3306.24

Frame	Ankle			Knee		
	Angle (deg)	Omega (deg/s)	Alpha (deg/s^2)	Angle (deg)	Omega (deg/s)	Alpha (deg/s^2)
153	122.7162	-245.96	-417.349	56.54115	117.4581	-3306.24
154	121.5694	-246.669	87.52497	57.05326	102.099	-3287.43
155	120.4197	-245.326	480.0564	57.49276	86.85089	-3251.8
156	119.2609	-242.415	775.4705	57.85484	71.75458	-3201.1
157	118.1326	-238.359	996.4763	58.15321	56.93813	-3138.68
158	117.043	-233.437	1175.202	58.39139	42.44395	-3066.86
159	115.9935	-227.772	1338.965	58.57045	28.3046	-2987.41
160	114.9557	-221.34	1500.64	58.67545	14.56933	-2901.62
161	113.9477	-214.159	1660.537	58.71654	1.243369	-2811.98
162	112.9502	-206.218	1806.264	58.68555	-11.6774	-2721.08
163	111.9992	-197.645	1930.754	58.59922	-24.1754	-2632.38
164	111.086	-188.532	2025.573	58.45418	-36.2815	-2547.53
165	110.2304	-179.057	2085.315	58.26076	-48.0098	-2468.71
166	109.417	-169.358	2106.951	58.0121	-59.3775	-2396.15
167	108.6574	-159.647	2086.46	57.71545	-70.4294	-2329.76
168	107.9196	-150.08	2023.564	57.35666	-81.1769	-2267.69
169	107.2352	-140.895	1921.569	56.95297	-91.6471	-2209.78
170	106.602	-132.24	1796.333	56.50564	-101.862	-2155.07
171	106.0164	-124.177	1666.454	56.01526	-111.841	-2103.21
172	105.4366	-116.65	1545.377	55.4633	-121.549	-2053.29
173	104.899	-109.664	1432.9	54.87065	-131.036	-2006.71
174	104.3896	-103.156	1328.762	54.23219	-140.321	-1963.9

Frame	Ankle			Knee		
	Angle (deg)	Omega (deg/s)	Alpha (deg/s^2)	Angle (deg)	Omega (deg/s)	Alpha (deg/s^2)
175	103.9239	-97.1251	1232.55	53.55771	-149.428	-1925.47
176	103.4846	-91.5325	1142.475	52.84121	-158.348	-1891.12
177	103.0764	-86.339	1063.312	52.08596	-167.125	-1860.62
178	102.687	-81.4854	999.0257	51.28794	-175.747	-1832.82
179	102.3192	-76.8923	953.2233	50.44959	-184.24	-1806.35
180	101.9553	-72.4412	925.4798	49.56188	-192.6	-1780.15
181	101.6226	-68.0789	920.6885	48.64	-200.857	-1754.13
182	101.3115	-63.6714	947.7917	47.68097	-208.984	-1727.38
183	101.0356	-59.0599	1009.79	46.69049	-217.008	-1699.15
184	100.7677	-54.0932	1101.822	45.65872	-224.839	-1668.63
185	100.5272	-48.6438	1214.337	44.59227	-232.525	-1636.13
186	100.3085	-42.6133	1341.179	43.48704	-240.045	-1601.08
187	100.1252	-35.9824	1467.198	42.34947	-247.402	-1563.06
188	99.97051	-28.7671	1583.282	41.17463	-254.572	-1521.03
189	99.86513	-21.0155	1693.579	39.97201	-261.567	-1474.61
190	99.79474	-12.8065	1783.996	38.73759	-268.318	-1423.13
191	99.7708	-4.25538	1840.115	37.4745	-274.831	-1365.92
192	99.7579	4.487307	1867.622	36.17235	-280.977	-1302.74
193	99.79385	13.30449	1875.557	34.84568	-286.83	-1233.73
194	99.87702	22.13973	1875.048	33.49428	-292.359	-1158.22
195	100.0106	30.94971	1863.124	32.12062	-297.542	-1075.95
196	100.1699	39.66105	1840.788	30.71883	-302.287	-986.629

Frame	Ankle			Knee		
	Angle (deg)	**Omega (deg/s)**	**Alpha (deg/s^2)**	**Angle (deg)**	**Omega (deg/s)**	**Alpha (deg/s^2)**
197	100.3783	48.24359	1809.745	29.2985	-306.622	-890.09
198	100.628	56.64483	1763.09	27.85781	-310.495	-785.633
199	100.9285	64.79869	1705.861	26.40292	-313.89	-670.381
200	101.2633	72.67546	1649.822	24.9348	-316.699	-541.16
201	101.6398	80.27845	1590.209	23.45668	-318.881	-394.847
202	102.0291	87.55549	1529.372	21.96757	-320.284	-228.299
203	102.453	94.53246	1466.738	20.47436	-320.862	-37.1957
204	102.8933	101.1847	1395.804	18.97459	-320.439	181.8723
205	103.3771	107.458	1303.078	17.4824	-318.964	431.0282
206	103.9039	113.1991	1164.972	16.00259	-316.293	710.8025
207	104.4673	118.1537	963.6653	14.53926	-312.276	1019.465
208	105.0343	121.9811	691.1183	13.09881	-306.752	1348.914
209	105.6185	124.3739	352.67	11.68822	-299.621	1713.541
210	106.202	125.04	-37.4094	10.31203	-290.812	2054.528
211	106.7936	123.8152	-456.064	8.981758	-280.274	2469.699
212	107.3571	120.6266	-873.224	7.70249	-268.005	2766.257
213	107.9118	115.5478	-1266.14	6.485533	-253.993	3245.522
214	108.4363	108.7154	-1623.89	5.339588	-238.501	3372.598
215	108.9322	100.2963	-1944.3	4.268334	-221.525	3941.331
216	109.3687	90.51509	-2204.1	3.280138	-203.924	3606.89
217	109.7654	79.68028	-2387.9	2.374695	-183.567	5482.612
218	110.1196	68.43348	-2400.07	1.587665	-153.377	6917.685

Frame	Ankle			Knee		
	Angle (deg)	Omega (deg/s)	Alpha (deg/s^2)	Angle (deg)	Omega (deg/s)	Alpha (deg/s^2)
219	110.4302	57.20914	-2362.24	0.942986	-127.986	3971.94
220	110.6693	46.85142	-2072.68	0.388184	-109.593	4145.164
221	110.868	37.34516	-1951.63	-0.07844	-91.5013	3590.097
222	111.0096	29.58827	-1442.19	-0.46667	-74.6855	3680.591
223	111.1293	20.8428	-2161.93	-0.77499	-57.8632	3523.663
224	111.2072	15.39178	-26.8235	-1.00584	-41.3392	3601.441
225	111.29	15.70502	23.48528	-1.15863	-24.6409	3571.908
226	111.3654	19.27877	1713.989	-1.23409	-7.94994	3621.062
227	111.4758	28.07883	1622.469	-1.23135	8.911369	3634.177
228	111.5994	30.12215	-559.632	-1.15023	25.90084	3662.065
229	111.729	27.50022	-457.322	-0.98924	43.01122	3684.413
230	111.8633	24.49451	-771.667	-0.74775	60.22991	3704.219
231	111.9959	21.38382	-542.671	-0.42515	77.55075	3720.726
232	112.1559	18.64805	-608.098	-0.01816	95.06412	3735.252
233	112.0705	16.03821	-489.37	0.454035	112.0751	3737.215
234	112.4466	13.6854	-496.226	1.039308	130.2647	3754.114
235	111.945	11.4298	-447.52	1.648149	146.3951	3734.611
236	112.8879	9.28494	-446.945	2.434626	165.9897	3768.392
237	111.4971	7.185287	-436.127	3.14931	180.0486	3710.168
238	113.7481	5.04841	-448.1	4.184222	202.7276	3790.418
239	110.1935	2.900337	-442.197	4.918622	211.6345	3645.64
240	116.7441	0.998717	-471.689	6.408632	244.5424	3888.304

Table B.2. The average reaction force of the ankle, and moment around ankle and knee

Frame	Reaction Force on Ankle		Ankle Moment	Knee Moment
	x-axis	z-axis		
1	-27.5823	185.0911	-3.11084	-3.52476
2	-36.5526	221.0756	-3.17352	-0.96376
3	-42.7264	237.9439	-3.19718	1.540985
4	-49.6155	262.4077	-3.18196	3.987611
5	-55.4444	281.208	-3.12807	6.374347
6	-61.3138	302.4229	-3.03576	8.699618
7	-66.535	320.925	-2.90533	10.96203
8	-71.5398	339.9033	-2.73712	13.16041
9	-76.073	357.4136	-2.5315	15.29386
10	-80.2758	374.5422	-2.28886	17.36183
11	-84.0769	390.7376	-2.00964	19.3642
12	-87.4884	406.1623	-1.69426	21.30146
13	-90.5126	420.8635	-1.34318	23.17482
14	-93.1374	434.836	-0.95686	24.98653
15	-95.3575	448.1023	-0.53573	26.74018
16	-97.1811	460.5237	-0.0802	28.44106
17	-98.7622	472.2044	0.409421	30.09421
18	-100.077	483.1157	0.932905	31.68741
19	-101.108	493.3267	1.490204	33.15003
20	-101.818	502.8196	2.081515	34.48014
21	-102.19	511.6633	2.70742	35.66977

Frame	Reaction Force on Ankle		Ankle Moment	Knee Moment
	x-axis	z-axis		
22	-102.199	519.7319	3.369081	36.7134
23	-101.88	527.1446	4.068577	37.61119
24	-101.189	533.8165	4.809413	38.36717
25	-100.136	539.8538	5.597089	38.98435
26	-98.7314	545.2371	6.438663	39.46508
27	-97.0068	549.8791	7.337017	39.80988
28	-94.9874	553.1107	8.286694	40.00998
29	-92.7607	555.1683	9.257526	40.07874
30	-90.3464	556.3342	10.24508	40.02023
31	-87.8029	556.6028	11.24488	39.83993
32	-85.1596	555.9242	12.25286	39.54518
33	-82.4811	554.4165	13.26501	39.14552
34	-79.794	552.0474	14.27724	38.65222
35	-77.1328	548.8733	15.28381	38.07728
36	-74.4895	544.7823	16.27575	37.43237
37	-71.8932	539.5691	17.23643	36.72778
38	-69.3327	533.6024	18.16647	35.97034
39	-66.7974	527.2073	19.06205	35.1624
40	-64.2608	520.25	19.91987	34.30234
41	-61.7216	512.9034	20.73706	33.38666
42	-59.1593	505.0962	21.51131	32.41344
43	-56.5934	497.0458	22.24101	31.38613

Frame	Reaction Force on Ankle		Ankle Moment	Knee Moment
	x-axis	z-axis		
44	-54.017	488.7489	22.92557	30.30984
45	-51.445	480.3428	23.56526	29.1901
46	-48.8825	471.8388	24.16131	28.03432
47	-46.3416	463.3212	24.71584	26.85065
48	-43.8238	454.7563	25.23183	25.64622
49	-41.3525	446.3134	25.71291	24.4266
50	-38.9362	438.046	26.16331	23.19599
51	-36.5785	429.9876	26.58778	21.95816
52	-34.2681	422.0321	26.99153	20.71816
53	-32.021	414.3916	27.38012	19.4822
54	-29.8302	407.0669	27.75944	18.25569
55	-27.701	400.1726	28.1357	17.04417
56	-25.6298	393.6867	28.51536	15.85334
57	-23.6187	387.6787	28.90516	14.68866
58	-21.6669	382.1145	29.312	13.5553
59	-19.7783	377.0682	29.74299	12.45819
60	-17.9475	372.4874	30.20526	11.4019
61	-16.1903	368.538	30.70587	10.39069
62	-14.5068	365.2019	31.25168	9.428366
63	-12.9012	362.5538	31.84922	8.518294
64	-11.3735	360.4992	32.50465	7.663407
65	-9.92646	359.1364	33.22368	6.866218

Frame	Reaction Force on Ankle		Ankle Moment	Knee Moment
	x-axis	z-axis		
66	-8.55898	358.4458	34.01156	6.128774
67	-7.27675	358.5021	34.87309	5.452608
68	-6.07746	359.2985	35.81251	4.838631
69	-4.96197	360.881	36.83353	4.287091
70	-3.92404	363.193	37.93921	3.797634
71	-2.95421	366.2782	39.13199	3.369444
72	-2.03888	369.9825	40.41365	3.00124
73	-1.1658	374.4573	41.78534	2.691244
74	-0.31671	379.699	43.24755	2.437105
75	0.528462	385.6973	44.80012	2.235878
76	1.390595	392.3409	46.44222	2.084036
77	2.289761	399.6931	48.17231	1.977576
78	3.247641	407.7016	49.98807	1.912129
79	4.281422	416.4123	51.88639	1.883082
80	5.404538	425.7016	53.86324	1.885593
81	6.637578	435.5953	55.91371	1.914699
82	7.994193	445.9117	58.03196	1.965588
83	9.497806	456.6931	60.21128	2.033877
84	11.17464	467.8401	62.44403	2.115768
85	13.05175	479.4156	64.72163	2.208179
86	15.15859	491.3742	67.03456	2.308807
87	17.52438	503.6578	69.37236	2.416239

Frame	Reaction Force on Ankle		Ankle Moment	Knee Moment
	x-axis	z-axis		
88	20.16126	516.0311	71.72367	2.53003
89	23.10295	528.5328	74.07626	2.650772
90	26.37074	541.071	76.41699	2.780073
91	29.97763	553.6331	78.73182	2.920538
92	33.92669	566.0553	81.00576	3.075586
93	38.22596	578.3941	83.22283	3.249321
94	42.85676	590.4751	85.36601	3.4464
95	47.81173	602.263	87.41735	3.671837
96	53.05111	613.5041	89.35801	3.93054
97	58.56233	624.2437	91.16846	4.226867
98	64.31627	634.3729	92.82869	4.564182
99	70.28077	643.769	94.31852	4.944591
100	76.40114	652.1379	95.61789	5.368842
101	82.65835	659.4997	96.70716	5.836489
102	88.99912	665.5814	97.56744	6.346166
103	95.40557	670.4055	98.18097	6.895888
104	101.8209	673.7728	98.53134	7.483172
105	108.2154	675.6126	98.60386	8.105083
106	114.5127	675.7069	98.38576	8.758197
107	120.6632	673.9933	97.86645	9.438508
108	126.5836	670.2513	97.03773	10.14121
109	132.2029	664.5492	95.89387	10.86051

Frame	Reaction Force on Ankle		Ankle Moment	Knee Moment
	x-axis	z-axis		
110	137.4373	656.8349	94.43186	11.58947
111	142.188	647.0345	92.6515	12.32007
112	146.3031	634.951	90.55563	13.04343
113	149.7275	620.7473	88.15034	13.75018
114	152.3614	604.4192	85.44517	14.43107
115	154.1246	586.1337	82.45337	15.07759
116	154.9172	565.9089	79.19192	15.68243
117	154.6793	543.9806	75.68164	16.2398
118	153.332	520.446	71.9471	16.74551
119	150.8486	495.5023	68.01642	17.19694
120	147.1962	469.2525	63.92107	17.59291
121	142.4167	442.0185	59.69545	17.93331
122	136.5426	413.9552	55.37646	18.2187
123	129.6767	385.3674	51.00286	18.44978
124	121.9057	356.3976	46.61455	18.62689
125	113.3879	327.3893	42.25178	18.74977
126	104.2586	298.5205	37.9543	18.81739
127	94.70564	270.1049	33.76052	18.82782
128	84.90328	242.3514	29.70662	18.77813
129	75.02747	215.4455	25.82577	18.66422
130	65.25938	189.5777	22.14747	18.48073
131	55.76713	164.9206	18.69697	18.22137

Frame	Reaction Force on Ankle		Ankle Moment	Knee Moment
	x-axis	z-axis		
132	46.67034	141.5218	15.49491	17.87933
133	38.15536	119.6635	12.55709	17.44801
134	30.33641	99.45671	9.894397	16.92184
135	23.29693	80.97032	7.512863	16.29727
136	17.09409	64.24869	5.41386	15.5737
137	11.7576	49.30682	3.59444	14.75446
138	7.283339	36.1092	2.047765	13.84746
139	3.67383	24.67344	0.763555	12.86566
140	0.884418	14.92574	-0.27149	11.82698
141	-1.1384	6.810528	-1.07327	10.75369
142	-2.48406	0.215706	-1.65989	9.671427
143	-3.25051	-4.96815	-2.05124	8.607775
144	-3.55723	-8.89362	-2.26866	7.590635
145	-3.5164	-11.6788	-2.33444	6.646414
146	-3.2444	-13.4776	-2.27148	5.798246
147	-2.84333	-14.4446	-2.10277	5.064445
148	-2.3947	-14.7293	-1.85105	4.457359
149	-1.95388	-14.4694	-1.53827	3.982734
150	-1.55473	-13.7976	-1.18522	3.639644
151	-1.2132	-12.8202	-0.8111	3.420936
152	-0.933	-11.6379	-0.43318	3.314105
153	-0.71038	-10.3374	-0.06651	3.302472

Frame	Reaction Force on Ankle		Ankle Moment	Knee Moment
	x-axis	z-axis		
154	-0.53692	-8.99094	0.276317	3.366559
155	-0.40222	-7.65833	0.585244	3.485499
156	-0.2962	-6.38546	0.852822	3.638392
157	-0.21351	-5.2116	1.074135	3.805484
158	-0.15035	-4.16237	1.246663	3.969123
159	-0.10419	-3.2521	1.370072	4.114463
160	-0.07207	-2.48509	1.445946	4.229909
161	-0.05056	-1.85721	1.477491	4.307326
162	-0.03628	-1.35518	1.469211	4.342045
163	-0.02651	-0.96719	1.42657	4.332683
164	-0.01935	-0.6745	1.355637	4.280823
165	-0.01396	-0.45937	1.262752	4.190607
166	-0.0099	-0.30445	1.15421	4.068119
167	-0.00686	-0.19537	1.035994	3.920671
168	-0.00458	-0.1195	0.913552	3.756072
169	-0.0029	-0.06927	0.791633	3.581907
170	-0.00174	-0.03744	0.674193	3.404914
171	-0.00102	-0.01841	0.564353	3.230512
172	-0.00059	-0.0078	0.464413	3.062521
173	-0.00032	-0.00258	0.37591	2.903102
174	-0.00014	-0.00022	0.299697	2.752889
175	-4.20E-05	0.000582	0.236052	2.611259

Frame	Reaction Force on Ankle		Ankle Moment	Knee Moment
	x-axis	z-axis		
176	-4.74E-06	0.000761	0.184787	2.476688
177	1.95E-06	0.000721	0.145358	2.34713
178	1.19E-06	0.000595	0.116958	2.220341
179	4.59E-07	0.000435	0.098605	2.094117
180	2.04E-07	0.00029	0.089201	1.966423
181	2.45E-07	0.000158	0.087591	1.835456
182	2.14E-07	6.97E-05	0.092598	1.699643
183	1.54E-07	2.28E-05	0.103051	1.557755
184	7.91E-08	4.24E-06	0.117797	1.40875
185	3.01E-08	4.70E-07	0.135708	1.251731
186	4.73E-09	-1.61E-07	0.155676	1.086028
187	0	-3.62E-07	0.176615	0.911274
188	0	-2.94E-07	0.197455	0.727744
189	0	-1.86E-07	0.217142	0.536822
190	0	-7.84E-08	0.234639	0.338749
191	0	-2.13E-08	0.248927	0.132577
192	0	-2.34E-08	0.25905	-0.0814
193	0	-1.20E-08	0.264093	-0.30361
194	0	-1.79E-09	0.263261	-0.53707
195	0	0	0.255962	-0.78873
196	0	0	0.241793	-1.06965
197	0	0	0.220542	-1.39235

Frame	Reaction Force on Ankle		Ankle Moment	Knee Moment
	x-axis	z-axis		
198	0	0	0.192245	-1.76827
199	0	0	0.156894	-2.20731
200	0	0	0.114427	-2.71606
201	0	0	0.064806	-3.28839
202	0	0	0.00826	-3.90848
203	0	0	-0.05445	-4.57271
204	0	0	-0.12213	-5.28479
205	0	0	-0.19322	-6.04954
206	0	0	-0.26673	-6.86653
207	0	0	-0.33913	-7.72769
208	0	0	-0.40905	-8.61742
209	0	0	-0.47547	-9.51434
210	0	0	-0.53755	-10.3926
211	0	0	-0.59465	-11.226
212	0	0	-0.6463	-11.9911
213	0	0	-0.69219	-12.6673
214	0	0	-0.73216	-13.2388
215	0	0	-0.7538	-13.6965
216	0	0	-0.77161	-14.0394
217	0	0	-0.78744	-14.2695
218	0	0	-0.80169	-14.3952
219	0	0	-0.81425	-14.4289

Frame	Reaction Force on Ankle		Ankle Moment	Knee Moment
	x-axis	z-axis		
220	0	0	-0.82483	-14.4106
221	0	0	-0.83316	-14.3329
222	0	0	-0.83897	-14.2087
223	0	0	-0.84203	-14.051
224	0	0	-0.84216	-13.9054
225	0	0	-0.83921	-13.7936
226	0	0	-0.83305	-13.7053
227	0	0	-0.82361	-13.6307
228	0	0	-0.81086	-13.5651
229	0	0	-0.79482	-13.5069
230	0	0	-0.7755	-13.4556
231	0	0	-0.75293	-13.4118
232	0	0	-0.72718	-13.3763
233	0	0	-0.69829	-13.3498
234	0	0	-0.66632	-13.3333
235	0	0	-0.63133	-13.3277
236	0	0	-0.59341	-13.3336
237	0	0	-0.55262	-13.3519
238	0	0	-0.50902	-13.3831
239	0	0	-0.4627	-13.4278
240	0	0	-0.41373	-13.4863

Appendix C: Motor Specification of GIM8008

Table C.1: Specification of MIT mini cheetah servo motor

Power Supply	**Voltage**	24 VDC ±10%
	Current	7A
Weight		600 g
Gear Rate		6 : 1
Output	**Maximum Torque**	15 Nm
	Maximum Speed	2000 RPM
	Maximum Power	200 W
Cooling Mode		Natural Cooling
Protection		Locked-rotor warning
Communication Interface		Smart CAN (CAN protocol, Rate 1M Hz)
Ambient Temperature		0-40°C

REFERENCES

1. O'Connor, J.J., et al., *The Geometry of the Knee in the Sagittal Plane.* Proceedings of the Institution of Mechanical Engineers, Part H: Journal of Engineering in Medicine, 1989. **203**(4): p. 223-233.
2. Forner-Cordero, A., et al., *Kinematics and dynamics of wearable robots.* Wearable robots: biomechatronic exoskeletons, 2008: p. 47-85.
3. Maeda, D., et al. *Muscle synergy analysis of human adaptation to a variable-stiffness exoskeleton: Human walk with a knee exoskeleton with pneumatic artificial muscles*. in *2012 12th IEEE-RAS International Conference on Humanoid Robots (Humanoids 2012)*. 2012.
4. Zhu, J., et al., *Unidirectional variable stiffness hydraulic actuator for load-carrying knee exoskeleton.* International Journal of Advanced Robotic Systems, 2017. **14**(1): p. 1729881416686955.
5. Anam, K. and A.A. Al-Jumaily, *Active exoskeleton control systems: State of the art.* Procedia Engineering, 2012. **41**: p. 988-994.
6. Zhang, L., et al., *Assistive devices of human knee joint: A review.* Robotics and Autonomous Systems, 2020. **125**: p. 103394.
7. Ergin, M.A. and V. Patoglu. *A self-adjusting knee exoskeleton for robot-assisted treatment of knee injuries*. in *2011 IEEE/RSJ International Conference on Intelligent Robots and Systems*. 2011. IEEE.
8. Khamar, M. and M. Edrisi, *Designing a backstepping sliding mode controller for an assistant human knee exoskeleton based on nonlinear disturbance observer.* Mechatronics, 2018. **54**: p. 121-132.
9. Mazumder, O., et al., *Development of series elastic actuator based myoelectric knee exoskeleton for trajectory generation and load augmentation.* Conference on Advances in Robotics ACM, 2015: p. 1-6.
10. Dos Santos, W.M., G.A. Caurin, and A.A. Siqueira, *Design and control of an active knee orthosis driven by a rotary series elastic actuator.* Control Engineering Practice, 2017. **58**: p. 307-318.
11. Han, Y., et al., *Research on a multimodal actuator-oriented power-assisted knee exoskeleton.* Robotica, 2017. **35**(9): p. 1906-1922.
12. Han, Y., B. Qi, and J. Yu, *Development and experimental study of elastic actuator for a power-assisted knee exoskeleton.* Robot, 2014. **36**(6): p. 668-675.
13. Han, Y., et al., *The Knee Exoskeleton Mechanical Leg Based on Multi-modal Elastic Actuator.* Jiqiren/Robot, 2017. **39**(4): p. 498-504.
14. Yali, H., et al., *The energy amplification characteristic research of a multimodal actuator.* International Journal of Advanced Robotic Systems, 2016. **13**(3): p. 93.
15. Félix, P., et al. *Powered knee orthosis for human gait rehabilitation: First advances*. in *2017 IEEE 5th Portuguese Meeting on Bioengineering (ENBENG)*. 2017. IEEE.
16. Figueiredo, J., et al. *Towards human-knee orthosis interaction based on adaptive impedance control through stiffness adjustment*. in *IEEE International Conference on Rehabilitation Robotics*. 2017.
17. Nikitczuk, J., et al. *Adaptive torque control of electro-rheological fluid brakes used in active knee rehabilitation devices*. in *Proceedings - IEEE International*

Conference on Robotics and Automation. 2006.

18. Weinberg, B., et al. *Design, control and human testing of an active knee rehabilitation orthotic device*. in *Proceedings - IEEE International Conference on Robotics and Automation*. 2007.
19. Jiang, J., et al. *Study on real-time control of exoskeleton knee using electromyographic signal*. in *Life System Modeling and Intelligent Computing: International Conference on Life System Modeling and Simulation, LSMS 2010, and International Conference on Intelligent Computing for Sustainable Energy and Environment, ICSEE 2010, Wuxi, China, September 17-20, 2010. Proceedings, Part III*. 2010. Springer.
20. Shan, H., et al. *Design and control of a wearable active knee orthosis for walking assistance*. in *2016 IEEE 14th International Workshop on Advanced Motion Control (AMC)*. 2016. IEEE.
21. el Zahraa Wehbi, F., et al. *Active impedance control of a knee-joint orthosis during swing phase*. in *2017 international conference on rehabilitation robotics (ICORR)*. 2017. IEEE.
22. Huang, T.-H., et al. *Design of a new hybrid control and knee orthosis for human walking and rehabilitation*. in *2012 IEEE/RSJ International Conference on Intelligent Robots and Systems*. 2012. IEEE.
23. Liu, L., et al. *EMG-driven model-based knee torque estimation on a variable impedance actuator orthosis*. in *2017 IEEE International Conference on Cyborg and Bionic Systems (CBS)*. 2017.
24. Rogers, E., et al. *A quasi-passive knee exoskeleton to assist during descent*. in *Wearable Robotics: Challenges and Trends: Proceedings of the 2nd International Symposium on Wearable Robotics, WeRob2016, October 18-21, 2016, Segovia, Spain*. 2017. Springer.
25. Shamaei, K., et al., *Design and evaluation of a quasi-passive knee exoskeleton for investigation of motor adaptation in lower extremity joints.* IEEE Transactions on Biomedical Engineering, 2014. **61**(6): p. 1809-1821.
26. Shamaei, K., P.C. Napolitano, and A.M. Dollar. *A quasi-passive compliant stance control Knee-Ankle-Foot Orthosis*. in *IEEE International Conference on Rehabilitation Robotics*. 2013.
27. Yuan, B., et al. *Designing of a passive knee-assisting exoskeleton for weight-bearing*. in *Intelligent Robotics and Applications: 10th International Conference, ICIRA 2017, Wuhan, China, August 16–18, 2017, Proceedings, Part II 10*. 2017. Springer.
28. Saleem, A., M.R. Khan, and S.M. Ahmmad. *A novel knee exoskeleton for overweight person*. in *2015 10th Asian Control Conference (ASCC)*. 2015.
29. Wu, S.-L. and H. Kazerooni. *Design of a passive exoskeleton knee to assist toe clearance*. in *Dynamic Systems and Control Conference*. 2017. American Society of Mechanical Engineers.
30. Chandrapal, M., X. Chen, and W. Wang, *Intelligent Assistive Knee Exoskeleton.* Mechatronics, 2013: p. 195-237.
31. Chaichaowarat, R., et al. *Passive knee exoskeleton using torsion spring for cycling assistance*. in *2017 IEEE/RSJ International Conference on Intelligent Robots and Systems (IROS)*. 2017. IEEE.
32. Chaichaowarat, R., J. Kinugawa, and K. Kosuge, *Unpowered Knee Exoskeleton*

Reduces Quadriceps Activity during Cycling. Engineering, 2018. **4**(4): p. 471-478.
33. Ranaweera, R., et al., *Development of A Passively Powered Knee Exoskeleton for Squat Lifting.* J. Robotics Netw. Artif. Life, 2018. **5**(1): p. 45-51.
34. Moyer, R., et al., *Combined versus individual effects of a valgus knee brace and lateral wedge foot orthotic during stair use in patients with knee osteoarthritis.* Gait & Posture, 2017. **54**: p. 160-166.
35. Kim, J.-H., et al., *Design of a knee exoskeleton using foot pressure and knee torque sensors.* International Journal of Advanced Robotic Systems, 2015. **12**(8): p. 112.
36. Celebi, B., M. Yalcin, and V. Patoglu. *AssistOn-Knee: A self-aligning knee exoskeleton*. in *IEEE International Conference on Intelligent Robots and Systems*. 2013.
37. Wang, J., et al., *Comfort-Centered Design of a Lightweight and Backdrivable Knee Exoskeleton.* IEEE Robotics and Automation Letters, 2018. **3**(4): p. 4265-4272.
38. Luo, Y., et al. *Design and control for a compliant knee exoskeleton*. in *2017 IEEE International Conference on Information and Automation, ICIA 2017*. 2017.
39. Shepherd, M.K. and E.J. Rouse, *Design and Validation of a Torque-Controllable Knee Exoskeleton for Sit-to-Stand Assistance.* IEEE/ASME Transactions on Mechatronics, 2017. **22**(4): p. 1695-1704.
40. Karavas, N., et al., *Tele-impedance based assistive control for a compliant knee exoskeleton.* Robotics and Autonomous Systems, 2015. **73**: p. 78-90.
41. Karavas, N.C., N.G. Tsagarakis, and D.G. Caldwell. *Design, modeling and control of a series elastic actuator for an assistive knee exoskeleton*. in *2012 4th IEEE RAS & EMBS International Conference on Biomedical Robotics and Biomechatronics (BioRob)*. 2012.
42. Karavas, N.C., et al. *A novel actuator with reconfigurable stiffness for a knee exoskeleton: Design and modeling*. in *Advances in Reconfigurable Mechanisms and Robots I*. 2012. Springer.
43. Lerner, Z.F., D.L. Damiano, and T.C. Bulea, *A lower-extremity exoskeleton improves knee extension in children with crouch gait from cerebral palsy.* Science Translational Medicine, 2017. **9**(404).
44. Lerner, Z.F., et al., *A Robotic Exoskeleton for Treatment of Crouch Gait in Children with Cerebral Palsy: Design and Initial Application.* IEEE Transactions on Neural Systems and Rehabilitation Engineering, 2017. **25**(6): p. 650-659.
45. Rifaï, H., et al., *Nested saturation based control of an actuated knee joint orthosis.* Mechatronics, 2013. **23**(8): p. 1141-1149.
46. Rifai, H., et al., *Toward Lower Limbs Functional Rehabilitation Through a Knee-Joint Exoskeleton.* IEEE Transactions on Control Systems Technology, 2017. **25**(2): p. 712-719.
47. Beyl, P., et al., *Safe and compliant guidance by a powered knee exoskeleton for robot-assisted rehabilitation of gait.* Advanced Robotics, 2011. **25**(5): p. 513-535.
48. Tung, W., et al. *On the design and control of exoskeleton knee*. in *Dynamic*

Systems and Control Conference. 2013. American Society of Mechanical Engineers.

49. Elliott, G.A., *Design and evaluation of a quasi-passive robotic knee brace: on the effects of parallel elasticity on human running.* Appl. Adv. Technol. Transp. Eng., 2012. **75**(2): p. 341-345.
50. Elliott, G., A. Marecki, and H. Herr, *Design of a clutch-spring knee exoskeleton for running.* Journal of Medical Devices, Transactions of the ASME, 2014. **8**(3).
51. Elliott, G., et al. *The biomechanics and energetics of human running using an elastic knee exoskeleton*. in *IEEE International Conference on Rehabilitation Robotics*. 2013.
52. Pagani, C.H.F., W. Potthast, and G.-P. Brüggemann, *The effect of valgus bracing on the knee adduction moment during gait and running in male subjects with varus alignment.* Clinical biomechanics, 2010. **25**(1): p. 70-76.
53. Pagani, C.H.F., et al., *Influence of a valgus knee brace on muscle activation and co-contraction in patients with medial knee osteoarthritis.* Journal of Electromyography and Kinesiology, 2013. **23**(2): p. 490-500.
54. Dollar, A.M. and H. Herr. *Design of a quasi-passive knee exoskeleton to assist running*. in *2008 IEEE/RSJ international conference on intelligent robots and systems*. 2008. IEEE.
55. Knaepen, K., et al., *Human–robot interaction: Kinematics and muscle activity inside a powered compliant knee exoskeleton.* IEEE transactions on neural systems and rehabilitation engineering, 2014. **22**(6): p. 1128-1137.
56. Tucker, M.R., et al. *Design of a wearable perturbator for human knee impedance estimation during gait*. in *2013 IEEE 13th International Conference on Rehabilitation Robotics (ICORR)*. 2013. IEEE.
57. Winter, D.A., *Biomechanics and motor control of human movement*. 2009: John Wiley & Sons.
58. Karavas, N., et al. *Tele-impedance based stiffness and motion augmentation for a knee exoskeleton device*. in *2013 IEEE international conference on robotics and automation*. 2013. IEEE.
59. Saccares, L., et al. *A novel human effort estimation method for knee assistive exoskeletons*. in *IEEE International Conference on Rehabilitation Robotics*. 2017.
60. Saccares, L., I. Sarakoglou, and N.G. Tsagarakis. *iT-Knee: An exoskeleton with ideal torque transmission interface for ergonomic power augmentation*. in *2016 IEEE/RSJ International Conference on Intelligent Robots and Systems (IROS)*. 2016.
61. Zhou, Z., et al. *Preliminary evaluation of gait assistance during treadmill walking with a light-weight bionic knee exoskeleton*. in *2016 IEEE International Conference on Robotics and Biomimetics (ROBIO)*. 2016. IEEE.
62. Kamali, K., A.A. Akbari, and A. Akbarzadeh, *Implementation of a trajectory predictor and an exponential sliding mode controller on a knee exoskeleton robot.* Modares Mech. Eng., 2016. **16**(6): p. 79-90.
63. Kardan, I. and A. Akbarzadeh, *Robust output feedback assistive control of a compliantly actuated knee exoskeleton.* Robotics and Autonomous Systems, 2017. **98**: p. 15-29.
64. Kardan, I. and A. Akbarzadeh. *Assistive control of a compliantly actuated single*

axis stage. in *4th RSI International Conference on Robotics and Mechatronics, ICRoM 2016*. 2017.
65. Witte, K.A., A.M. Fatschel, and S.H. Collins. *Design of a lightweight, tethered, torque-controlled knee exoskeleton*. in *IEEE International Conference on Rehabilitation Robotics*. 2017.
66. Sridar, S., et al. *Development of a soft-inflatable exosuit for knee rehabilitation*. in *2017 IEEE/RSJ International Conference on Intelligent Robots and Systems (IROS)*. 2017.
67. Liao, Y., Z. Zhou, and Q. Wang. *BioKEX: A bionic knee exoskeleton with proxy-based sliding mode control*. in *2015 Ieee International Conference on Industrial Technology (Icit)*. 2015. IEEE.
68. Li, B., et al., *Biomechanical design analysis and experiments evaluation of a passive knee-assisting exoskeleton for weight-climbing.* Industrial Robot: An International Journal, 2018.
69. Jun, S., et al. *Compliant knee exoskeleton design: parallel coupled compliant plate (PCCP) mechanism and pennate elastic band (PEB) spring*. in *International Design Engineering Technical Conferences and Computers and Information in Engineering Conference*. 2014. American Society of Mechanical Engineers.
70. Malcolm, P., et al., *Bi-articular knee-ankle-foot exoskeleton produces higher metabolic cost reduction than weight-matched mono-articular exoskeleton.* Frontiers in neuroscience, 2018. **12**: p. 69.
71. Kong, K., J. Bae, and M. Tomizuka, *A compact rotary series elastic actuator for human assistive systems.* IEEE/ASME transactions on mechatronics, 2011. **17**(2): p. 288-297.
72. Pratt, J.E., et al. *The RoboKnee: an exoskeleton for enhancing strength and endurance during walking*. in *IEEE International Conference on Robotics and Automation, 2004. Proceedings. ICRA'04. 2004*. 2004. IEEE.
73. Ma, H., et al. *Design and control of a powered knee orthosis for gait assistance*. in *2013 IEEE/ASME International Conference on Advanced Intelligent Mechatronics*. 2013. IEEE.
74. Ma, H., et al., *Design and testing of a regenerative magnetorheological actuator for assistive knee braces.* Smart Materials and Structures, 2017. **26**(3): p. 035013.
75. Chen, B., et al., *Knee exoskeletons for gait rehabilitation and human performance augmentation: A state-of-the-art.* Mechanism and Machine Theory, 2019. **134**: p. 499-511.
76. Rose, J. and J.G. Gamble, *Human walking. Lippincott Williams & Wilkins.* Philadelphia [Google Scholar], 2006.
77. Masouros, S.D., A.M.J. Bull, and A.A. Amis, *(i) Biomechanics of the knee joint.* Orthopaedics and Trauma, 2010. **24**(2): p. 84-91.
78. Dixit, S., et al., *Management of patellofemoral pain syndrome.* American family physician, 2007. **75**(2): p. 194-202.
79. Bertomeu, J.M.B., et al., *Development of a hinge compatible with the kinematics of the knee joint.* Prosthetics and orthotics international, 2007. **31**(4): p. 371-383.
80. Grimmer, M., et al., *Stance and swing detection based on the angular velocity of lower limb segments during walking.* Frontiers in neurorobotics, 2019: p. 57.

81. Javanfar, A. and M. Bamdad, *A developed multibody knee model for unloading knee with cartilage penetration depth control.* Proceedings of the Institution of Mechanical Engineers, Part H: Journal of Engineering in Medicine, 2022. **236**(10): p. 1528-1540.
82. Mokri, C., M. Bamdad, and V. Abolghasemi, *Muscle force estimation from lower limb EMG signals using novel optimised machine learning techniques.* Medical & Biological Engineering & Computing, 2022. **60**(3): p. 683-699.
83. Rattanasak, A., et al., *Real-Time Gait Phase Detection Using Wearable Sensors for Transtibial Prosthesis Based on a kNN Algorithm.* Sensors, 2022. **22**(11): p. 4242.
84. Chen, B., et al., *Computer Vision and Machine Learning-Based Gait Pattern Recognition for Flat Fall Prediction.* Sensors, 2022. **22**(20): p. 7960.
85. Robertson, D., et al., *Research methods in biomechanics 2nd ed*. Boston (USA): Human Kinetics. 2013.
86. Quarteroni, A., F. Saleri, and P. Gervasio, *Scientific computing with MATLAB and Octave*. Vol. 3. 2006: Springer.
87. Fornberg, B., *Generation of finite difference formulas on arbitrarily spaced grids.* Mathematics of computation, 1988. **51**(184): p. 699-706.

VITA

NAME	Khemwutta Pornpipatsakul
DATE OF BIRTH	24 March 1999
PLACE OF BIRTH	Bangkok
INSTITUTIONS ATTENDED	Department of Mechanical Engineering, Chulalongkorn University
HOME ADDRESS	50/36, Bang Bon 3 rd., Soi Phet Kasaem 69, Nongkhaem Sub District, Nong Khaem District, Bangkok, Thailand Postcode: 10160
PUBLICATION	2023 - Pornpipatsakul, K.; Ajavakom, N. Estimation of Knee Assistive Moment in a Gait Cycle Using Knee Angle and Knee Angular Velocity through Machine Learning and Artificial Stiffness Control Strategy (MLASCS). Robotics 2023, 12, 44. https://doi.org/10.3390/ robotics12020044 2022 - T. Micaraseth, K. Pornpipatsakul, R. Chancharoen and G. Phanomchoeng, "Coffee Bean Inspection Machine with Deep Learning Classification," 2022 International Conference on Electrical, Computer, Communications and Mechatronics Engineering (ICECCME), Maldives, Maldives, 2022, pp. 1-5, doi: 10.1109/ICECCME55909.2022.9987835.